Numerical Investigation of the Performance of a Hydrokinetic Turbine

By

Xiaoran Zha

Undergraduate Research Thesis

The Ohio State University

2021

Advisor: Dr. Clarissa Belloni

Abstract

As the usage of electricity increases, people are seeking ways to generate electricity in an environmentally friendly way. According to a study done by BP [1], the global hydroelectricity consumption in 2019 was 948.8 Million tones of oil equivalent, including hydrokinetic power. Compared to traditional hydropower, hydrokinetic power has advantages such as considerably less construction work and a lower environmental impact, so it is essential to find an efficient way to utilize hydrokinetic energy. The main purpose of this research is to simulate a three-dimensional Computational Fluid Dynamics (CFD) model of a Schottel SIT tidal turbine by using the Finite Volume Method (FVM). The software ANSYS Fluent is used to simulate the working condition of the hydrokinetic turbine and provide accurate power predictions under various working conditions. The first simulation is conducted using the same working conditions as the on-site test of the same turbine to get similar performance characteristics such as torque and power. The sliding mesh method is used to better simulate the rotating working condition of the blades. This step is also important to examine the simulation setups, such as mesh sizes and time-step sizes. Finer meshes are created where turbulence may generate to make more accurate power predictions. The next step is to perform CFD simulations using different flow speeds and RPM and find the working condition that can produce maximum power, which will be helpful for future on-site tests on the SIT turbine and other turbines that use similar blade design to save the test time and cost.

Acknowledgement

First of all, I would like to thank my advisor Dr. Clarissa Belloni for providing the opportunity to do this research. Her generous guidance along with my research encouraged me when dealing with the difficulties and finally finished the research. It is truly a privilege to be her student because I didn't exclusively learn CFD related knowledge from her, I also learned the whole procedure of doing a research, and I could not thank her enough.

I would also thank Dr. Zhenyu Wang for his assistance in this research and being the examiner of this research. His deep understanding of CFD simulations and rich experience on Fluent are essential assistance for my research. Without his help this study will never finish. His suggestions during my oral defense helped me to better illustrate my results and to write a concise report.

I also appreciate the assistance provided by Mr. Rodrigo Auza Gutierrez from SimCenter for his suggestion during my 3D modeling and mesh generation at the beginning of my research. I also would like to thank him for his advice on the general research direction before I have a solid plan for each step.

Finally, I would like to thank Ohio Supercomputer Center (OSC) for providing their platform. It would be impossible to finish the simulation in time without operating on the Owens Supercomputer.

Table of Contents

Nomenclature

ρ	Fluid Density
t	Time
∇	Nabla operator
U	Flow velocity
τ	Stress tensor
F	External body force
μ	Dynamic viscosity
I	Unit tensor
V	Control volume
ν	Dynamic viscosity
W	Relative velocity
Cf	Skin friction coefficient
Re	Reynolds number
y+	Near wall function
P	Power
T	Torque
ω	Rotational speed
λ	Tip speed ratio (TSR)
r	Radius
#	Quantity
Cp	Power coefficient
$\emptyset$	Scalor

Introduction

Section 1.1 gives a brief introduction to the current situation and future prediction of hydrokinetic power as a type of renewable energy. The details of the turbine used in this study and its on-site test data are presented in section 1.2. The purposes and steps of this research are described at the end of this chapter.

1.1 Introduction to Hydro Power

Energy consumption in the world increased rapidly in recent years while the pollution and greenhouse gas emission caused by burning fossil fuels is raising more concerns globally. As a result, the demand for renewable energy will keep growing at least until 2050. Among all the types of renewable energy, hydropower is most widely used, which provides 16% of the total energy produced [1]. Nowadays, the majority portion of hydropower is traditional hydropower plants, which require massive resources for the construction of dams to block rivers and create a reservoir, and then the water flow goes through volute channels to run the turbines, typically Francis and Kaplan turbines. The constructed hydropower plant can be used for purposes like power generation, flow control, and water supplies, but their disadvantages restricted their locations and numbers. From the geology perspective, the weight of the reservoir gives massive pressure to the sediment, so the geological assessments before hydro plant construction are extremely long and strict, and that restricted the possibility to be applied widely, especially in the less developed regions. The maintenance cost is also not negligible, which includes the dam, the river sediments, and environmental protection. Overall, the traditional hydropower plants are multifunction civil constructions, and power generation is only one of the purposes. To increase the amount of hydro renewable energies, a more environmental-friendly method is necessary for future installations.

As for hydrokinetic energy, the method is to generate power using the kinetic energy from moving flows, such as the rivers and tides. Hydrokinetic energy does not require potential energy from the dam and reservoirs, thereby simplifying construction. The 2019 Annual Report from Ocean Energy System organization shows the cumulative energy generated from hydrokinetic sources in 2019 was 50 GWh [2], and the hydrokinetic installed capacity in 2050 is projected to be 300 GW [3]. Hence, the effort is being placed on the further development of hydrokinetic devices.

1.2 Hydrokinetic Turbines

The working mode of hydrokinetic energy is relatively easy, and there are some variations on the different modes of hydrokinetic turbines. In-stream hydrokinetic turbines can be classified as axial flow devices and cross flow devices. The more developed hydrokinetic turbines are axial flow turbines, which functions similarly to wind turbines. The principles behind wind turbines and axial hydrokinetic turbines are similar, but due to the high density of water comparing to air, the size of hydrokinetic turbines is significantly smaller than wind turbines.

1.2 Turbine Model in This Study

The turbine that being studied is the Schottel Instream Turbine (SIT), which is a three-blade axial flow hydrokinetic turbine, with the rotor mounted downstream of the nacelle. It has a blade radius of 2 meters and a rated power of 70 kW. The manufacturer Schottel conducted field measurements of this turbine at Queen's University Belfast's tidal site at Strangford Lough, NI. Power generated in flows from 0 to 2.5 m/s were measured and the maximum power reported is 19 kW [6]. Figure 1.2 is the schematic of the test setup. The results of the full-scale models gave experiment power data for simulation validations.

A towing test was done on a 1:8 scale model of the SIT turbine as shown in figure 1.4 in the University of Siegen to do cavitation inception tests [2]. The results were used to find the tip speed ratio in simulations, which ultimately determined the initial angular velocity of the turbine.

The installation of the turbines is a 4-Turbine array set on the PLAT-1 platform as figure 1.3. Tests were done to demonstrate the system's viability by placing the mooring turbine for several months near the Falls of Lora in Western Scotland in the UK, and the overall rated electric power of the complete platform is 280 kW[3].

Figure 1.1 Schottel Instream Turbine [7]

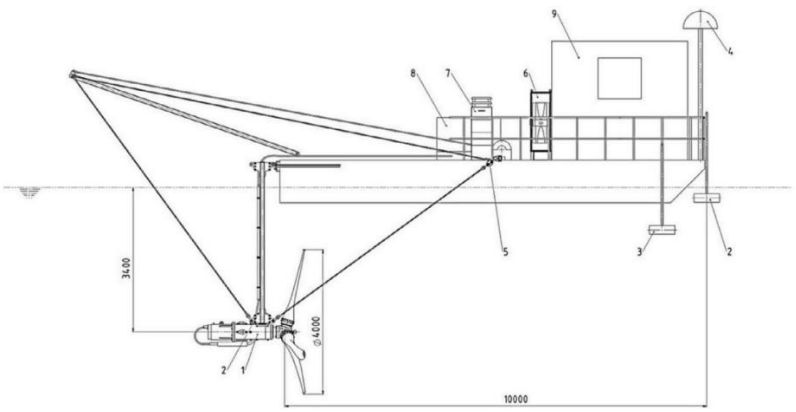

Fig. 5. Schematic of barge with turbine in testing position – (1) TEC, (2) ADP, (3) ADV & sonar, (4) DGPS, (5) load cell, (6) electrical cabinet, (7) resistor bank, (8) generator, (9) operations room.

Figure 1.2 Field testing schematic [6]

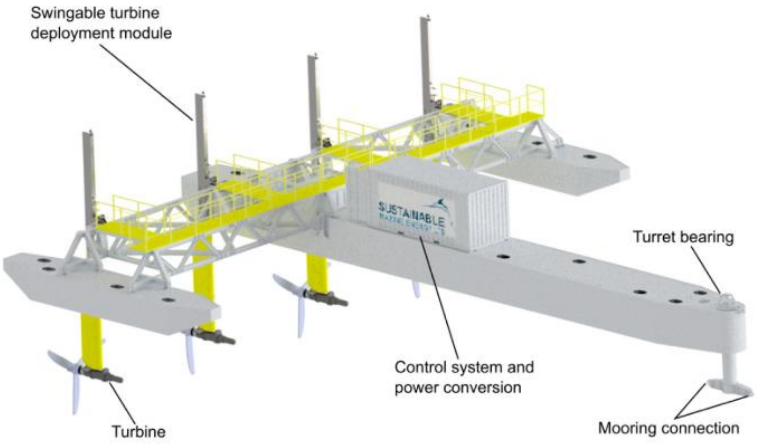

Figure 1.3 PLAT-1 4 turbine installation platform [3]

Figure 1.4 1:8 scale bronze model of SIT for towing test [4]

1.3 Research Objectives

The main objectives of this research are to accurately predict the performance and optimal operating condition of the SIT hydrokinetic turbine through CFD modeling. The first step is to run simulations with conditions similar with those employed in the open water tests by the manufacturer Schottel. These are used to validate the CFD model and fine tune mesh size as well as other factors of the numerical solution such as number and size of timesteps. As part of this process a grid convergence study is performed which is a necessary step in CFD simulations to ensure the meshes reached an optimal value. The following stage is to

run simulations using different flow speeds and rotational velocity, to find the condition that generates the most power, and maximum efficiency.

1.4 Thesis Layout

This thesis is split into the following parts:

Chapter 2 is the introduction of the mathematical model behind CFD simulations, including the governing equations, turbulence models, sliding mesh method and finite volume method (FVM).

Chapter 3 is the Methodology and the results, which includes setups like the turbine geometry, flow domain, numerical mesh, and simulation setups. The chapter also includes simulation convergence and grid convergence study and flow field analysis.

Chapter 4 shows the flow field analysis and the comparison between the simulation results and the field measurement data provided by the turbine manufacturer.

Finally, Chapter 5 draws a conclusion to this study and suggests future work that would the logical next steps based on this work.

Chapter 2. Basic Mathematical Models of CFD

For modern commercial CFD software such as ANSYS Fluent, users can switch models instantly without writing codes to solve different Partial Differential Equations, but it is important to know the principles of different models so that proper options can be chosen to fit different scenarios. The governing equations of CFD are introduced in section 2.1, and the theory background of sliding mesh and the turbulence model chosen are briefly introduced in section 2.2 and 2.3.

2.1 Governing Equations

There are two methods to describe the movement of the fluids, the Lagrangian description and the Eulerian method. In the Lagrangian method, individual fluid particles are traced and their properties like velocities and positions are described as functions of time. While in the Eulerian method, a control volume is defined first and the properties of the fluids going in and out of the control volume is considered regardless of the properties of individual fluid particles. In a typical CFD simulation, a flow field is defined first, and fluids are assumed to be a continuous flow entering and leaving the flow domain. As a result, Eulerian method is generally used in CFD simulations. For a control volume, three conservation laws are the governing equations for the analysis: mass conservation (continuity equation), momentum conservation, and energy conservation [8].

Mass conservation equation can be written as the form:

$$\frac{\partial \rho}{\partial t} + \nabla \cdot (\rho \vec{v}) = 0 \tag{2.1}$$

Where ρ = fluid density, t = time, ∇ = nabla operator, v = flow velocity.

The momentum conservation equation, also known as the Navier-Stokes equation can be described as the form:

$$\frac{\partial}{\partial t}(\rho\vec{U}) + \nabla \cdot (\rho\vec{U}\vec{U}) = -\nabla p + \nabla \cdot (\vec{\tau}) + \rho g + \vec{F} \quad (2.2)$$

Where U = flow velocity, τ = stress tensor, ρg= gravitational body force, and F =external body force. The stress tensor can be written as:

$$\vec{\tau} = \mu\left[(\nabla\vec{U} + \nabla\vec{U}^T) - \frac{2}{3}\nabla \cdot \vec{U}I\right] \quad (2.3)$$

Where μ = dynamic viscosity, I = unit tensor [9].

In this research, the simulated flow is incompressible, so ρ is a constant in momentum conservation equation. The gravitational body force is neglected because the tidal flow that the turbine deals with is a parallel flow comparing to the size of the flow domain. Finally, there are no external force on the control volume so the externa body force can be considered as 0 as well.

In this study, the energy changes in the flow domain are considered as negligible comparing to the kinetic energy of the fluids, so energy conservations are not considered when analyzing the fluid properties in the control volume.

2.2 Turbulence Models

Turbulence models are mathematical models to predict turbulences. Since this study focuses on accurate prediction of turbine performance, it is important to choose the correct turbulence model for a simulation of the water flow close to the blades and the wake of the turbine, while not taking too much computational resources. One proven and efficient model is the Reynolds Averaged Navier Stokes equations (RANS), where Reynolds Averaging Method is a way that substitutes the exact solution variables of Navier-Stokes equations with the mean and fluctuating components:

$$\emptyset = \overline{\phi} + \phi' \tag{2.4}$$

Where ϕ represents a scalar such as pressure or energy [9]. The Cartesian tensor form of RANS equations can be written as:

$$\frac{\partial\,\rho}{\partial t} + \frac{\partial}{\partial x_i}(\rho u_i) = 0 \tag{2.5.1}$$

$$\frac{\partial}{\partial t}(\rho u_i) + \frac{\partial}{\partial\, x_j}(\rho u_i u_j) = -\frac{\partial p}{\partial x_i} + \frac{\partial}{\partial x_j}\mu\left(\frac{\partial u_i}{\partial x_j} + \frac{\partial u_j}{\partial x_i}\right) + \frac{\partial}{\partial x_j}\left(-\rho\overline{u_i' u_j'}\right) \tag{2.5.2}$$

Where u is the velocity, and $-\rho\overline{u_i' u_j'}$ are the Reynold stresses [9]. The Reynolds stresses are molded using Boussineq hypothesis to relate Reynold stresses to the mean velocity gradients. Three models employed Boussineq hypothesis: Spalart-Allmaras model, $k-\epsilon$ model, and - $k-\omega$ model. For low-speed (<< Mach 1) and incompressible flow, $k-\epsilon$ model and $k-\omega$ model are widely employed, where k = turbulent kinetic energy, ϵ = turbulence dissipation rate, and ω = specific dissipation rate. Dissipation means the conversion from kinetic energy to thermal internal energy, and ω is the conversion rate per unit volume and time. $k-\omega$ model predicts well near wall areas, and $k-\epsilon$ model predicts well far from the walls. For this research, both near wall and far from wall regions are important to analyze the turbine performance, but the near wall areas are more essential when monitoring the torque applied to the blade. As a result, the $k-\omega-SST$ model is employed, which focuses more on the far from wall regions than the standard $k-\omega$ model, while maintaining the near wall treatment.

2.3 Sliding Mesh Method

In this research, the rotating blades are a key part of performance analysis, and this involves the move of cell zone boundaries. The dynamic mesh model is a method that allows the movement of boundaries over time, which is a transient simulation process. The conservation equation for a general scalar is:

$$\frac{d}{dt}\int_V \rho\phi \, dV = \frac{(\rho\phi V)^{n+1} - (\rho\phi V)^n}{\Delta t} \tag{2.6.1}$$

And the control volume V follows the relationship:

$$V^{n+1} = V^n + \frac{dV}{dt}\Delta t \tag{2.6.2}$$

The dynamic mesh can be considered as sliding mesh if the following restrictions are met. Firstly, the boundaries and the cells are not deformed during mesh movement; secondly, the mesh zone movement can be linked by non-conformal interfaces; and finally, the interfaces dynamically updated as the mesh moves. The mesh movement in this research meets with all the conditions. The rotation of the blades will not deform the boundaries and the cells around them, and the fluid flows between different cell zones [9]. The conservation equation of the sliding mesh can be written as:

$$\frac{d}{dt}\int_V \rho\phi \, dV = \frac{[(\rho\phi)^{n+1} - (\rho\phi)^n]\, V}{\Delta t} \tag{2.7}$$

Chapter 3. Methodology

The original geometry is a single blade, and the turbine is the combined geometry of three same blades. The turbine has a radius of 2 meters and a hub radius of 0.19m. However, the wall geometry near the hub was deemed too complex to be meshed as is and hence the radius of the hub was increased to cover some of the complex. Given that little torque is produced at the hub this was deemed appropriate. The finalized turbine geometry has a hub radius of 0.25m.

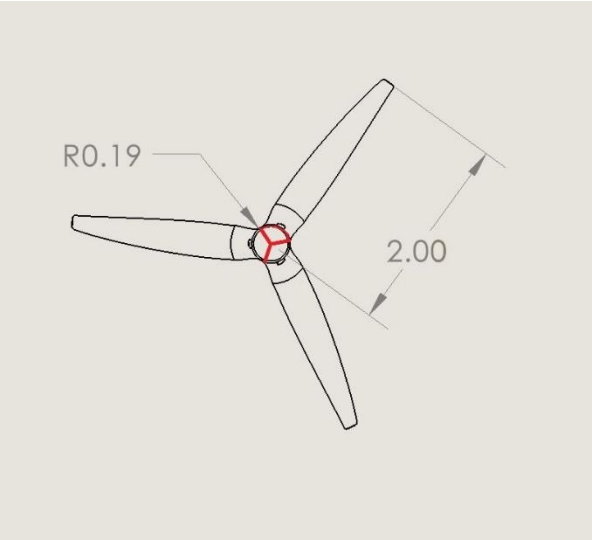

Figure 3.1 Original Blade Geometry

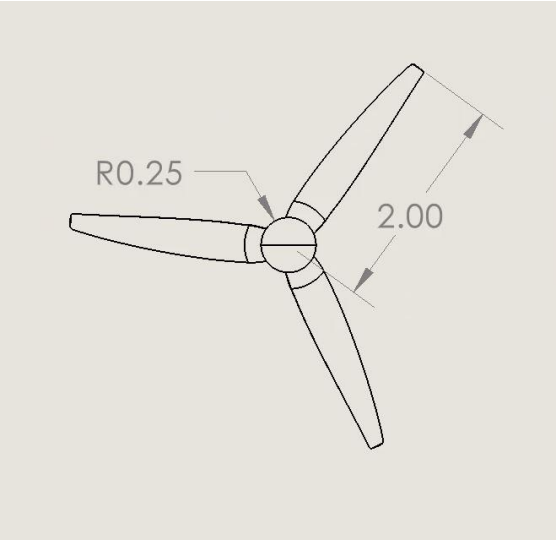

Figure 3.1 Final Blade Geometry

3.1 Turbine Geometry and Flow Domain Setup

The flow domain has a width of 20 meters (5 rotor diameters), a height of 14 meters (3.5 rotor diameters), and a length of 26 meters (6.5 rotor diameters). The upstream length is 6 meters and the downstream is 20 meters. The center of the turbine hub is at the origin of the coordinate system, and a cylindrical geometry is created around the turbine blades as sliding mesh cell zone. The cylinder has a radius of 2.2 meters and a length of 0.73 meters, which leaves a 0.2-meter gap between blade tips and the cylinder surface for meshing. Figure 3.3 shows the details of different geometry sizes and functions. The larger influence geometry on

the left refines the mesh size in the volume to capture the turbulence at the downstream of the blades.

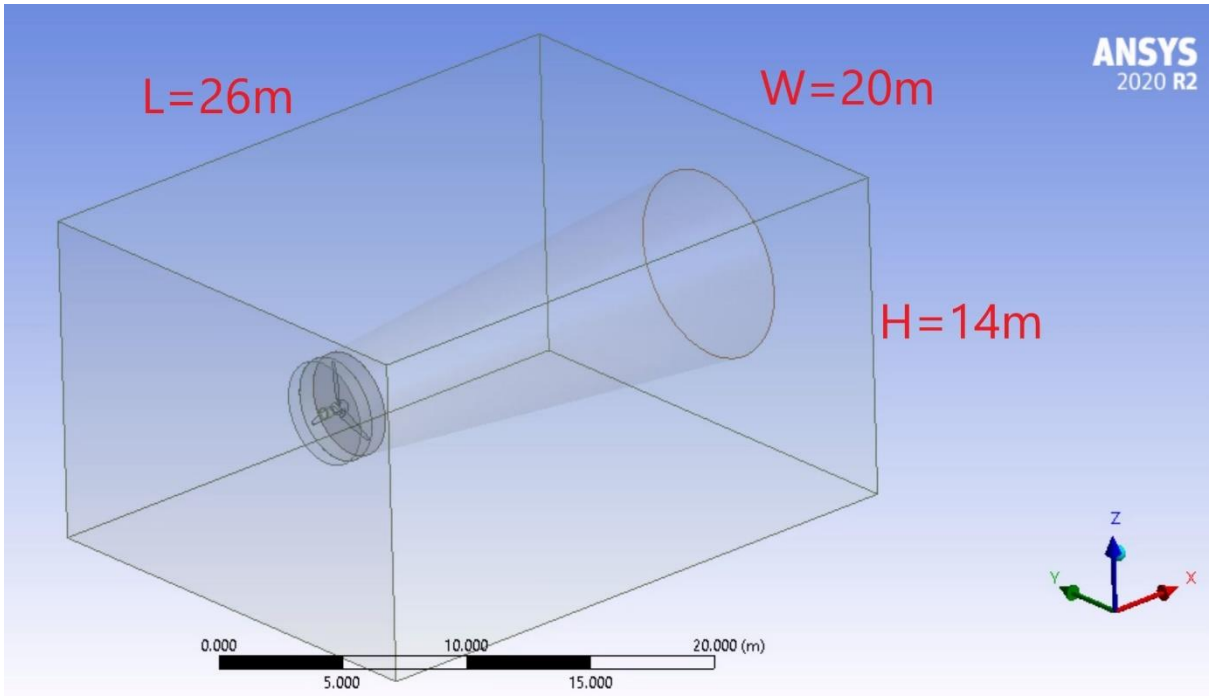

Figure 3.2 Flow Domain Geometry

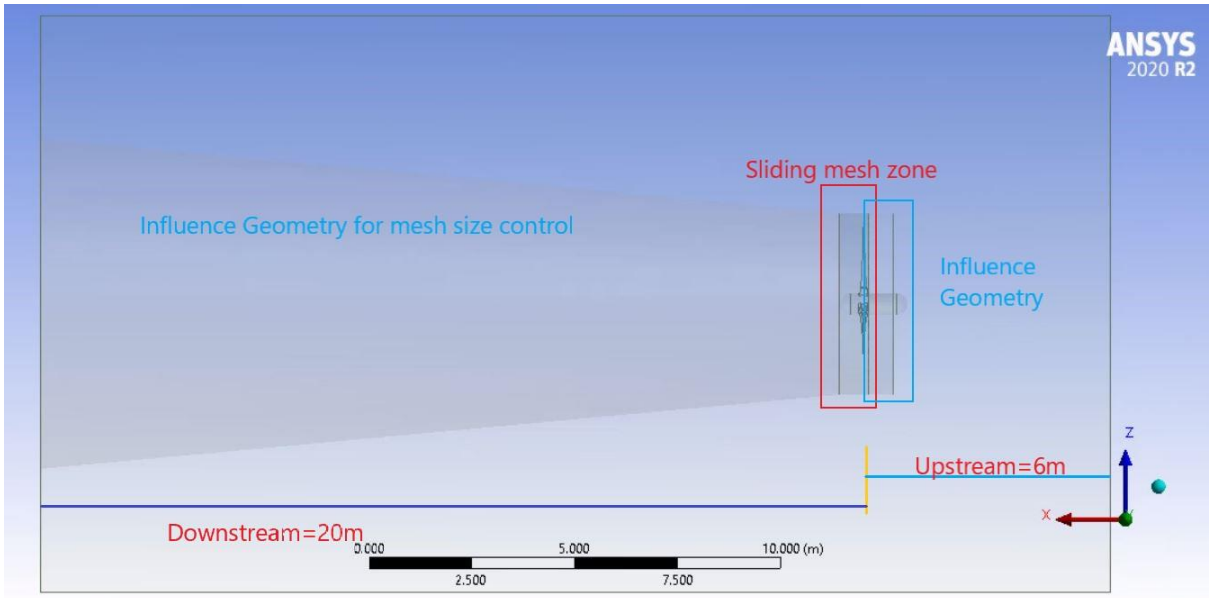

Figure 3.3 Geometry with notations

3.2 Numerical Mesh

The mesh is generated using ANSYS Meshing. Most part of the mesh is automatically generated using a maximum size control of 1 meter, while regions of higher importance have additional control on the mesh size for capturing more specific flow. The highest resolution can be found in the sliding mesh region. The meshes inside the surfaces are not shown in the wireframe figure, Fig 3.4, which will be detailed later.

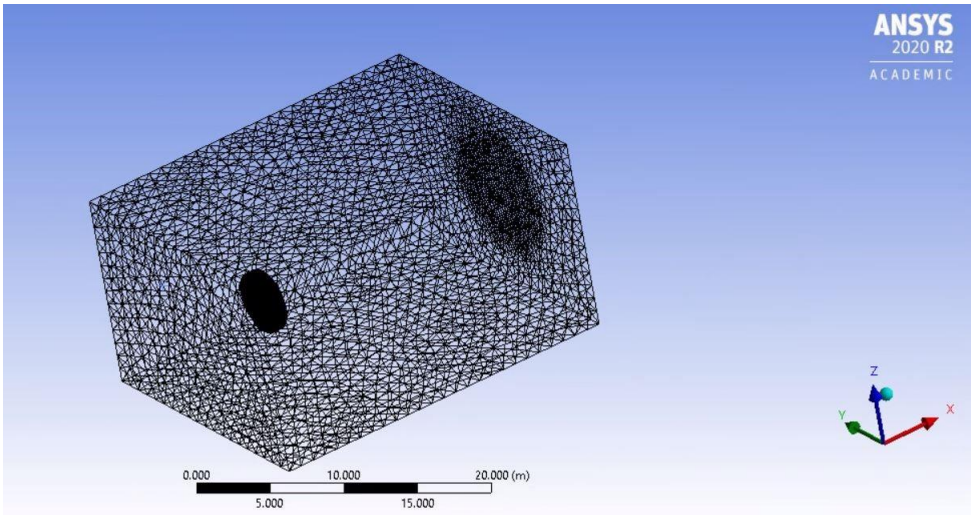

Figure 3.4 Wireframe mesh overview

For the wake region behind the turbine where large gradients of velocities occur and high turbulence is expected, the maximum mesh element size is set as 0.3 m, as shown in figure 3.5.

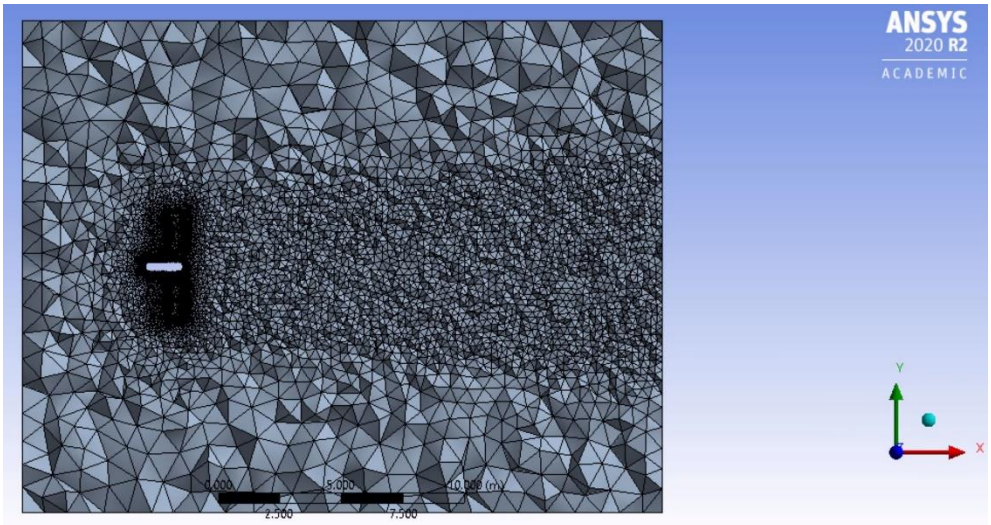

Figure 3.5 Section Overview

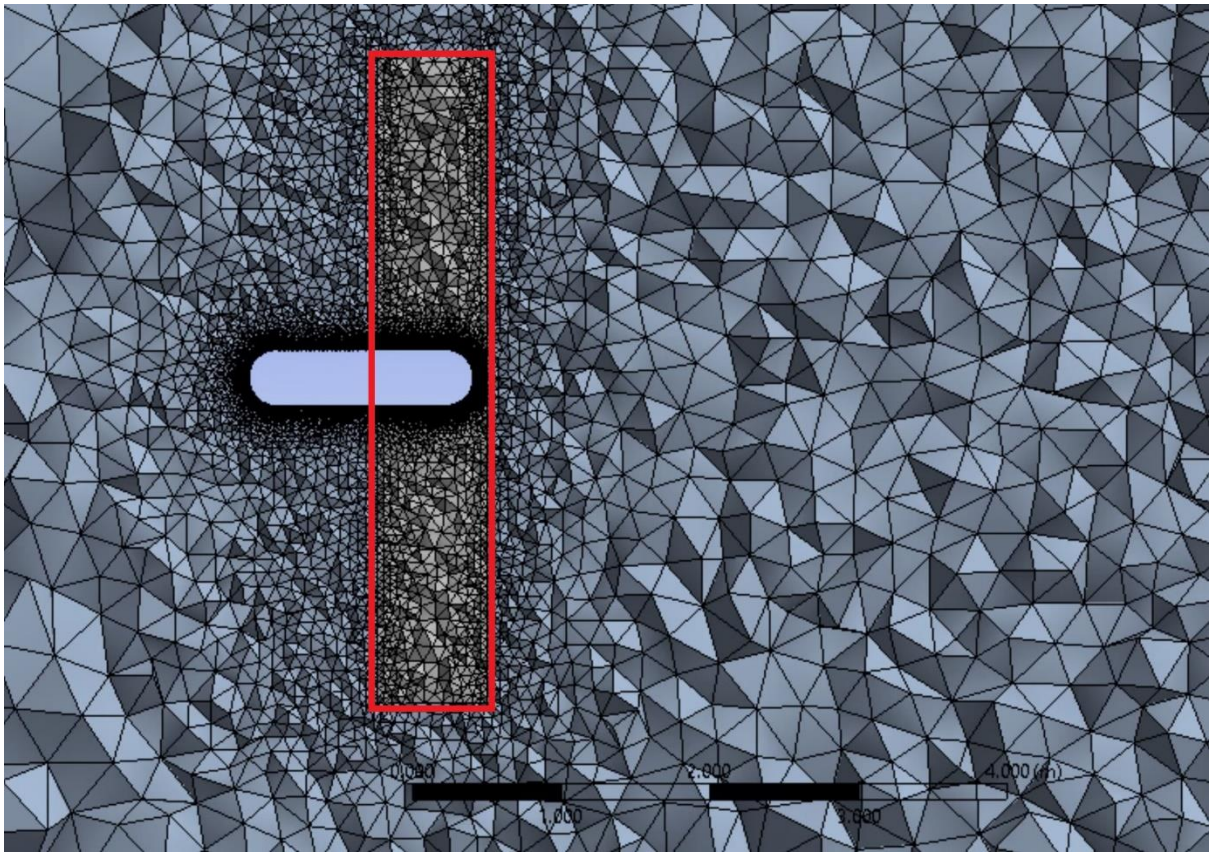

Figure 3.6 Face sizing

Further refinement was used for the rotating mesh region. Figure 3.6 shows the smooth mesh size transition between sliding mesh region (red box) and its surrounding stationary mesh region, which is achieved by the face sizing on the interfaces between these mesh zones. The face mesh element size is set to be 0.05 meter.

When the fluid flows through the surface of the turbine, the non-slip condition of fluid causes the distortions of the fluid particles, and lead to a growth of the boundary layer, which will ultimately become turbulent. In order to properly capture the turbulent flow within the boundary layer using a turbulence model, it is essential to generate a highly resolved boundary layer mesh, often referred to as inflation layer. In this portion of the mesh prism layers are introduced, often of the order to 4-10 layers, for this study 5 layers are chosen. The

first layer height is essential when using the $k-\omega-SST$ model to capture the near wall areas.

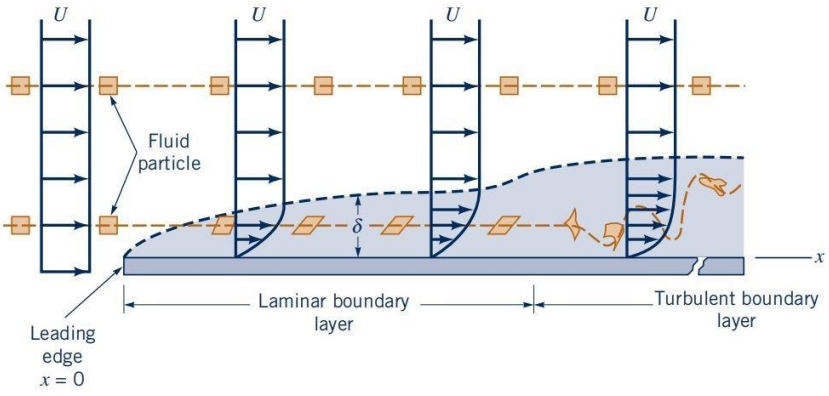

Figure 3.7 Boundary layer development [11]

The y+ value is generally used to describe the adequacy of the first layer cell height and for $k-\omega-SST$ model should be close to 1 [10] with y+ defined by:

$$y^+ = \frac{y_p \mu_t}{\nu} \tag{3.1}$$

Where y_p is the half of the first layer mesh height, and ν is the dynamic viscosity of the fluid. μ_t can be written as:

$$\mu_t = W\sqrt{C_f/2} \tag{3.2}$$

Where W is the relative velocity that flows through the cross section of the turbine blade at 2/3 span.

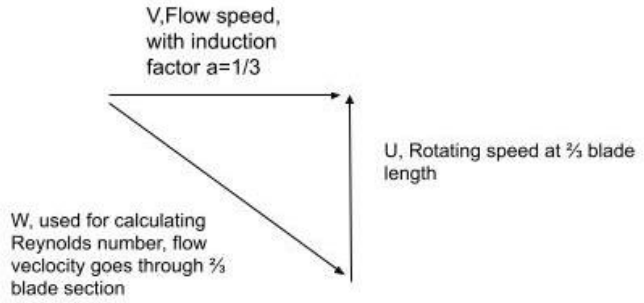

Figure 3.8 Velocity triangle for the W calculation

The skin friction coefficient Cf can be estimated as:

$$C_f = \frac{0.064}{Re^{\frac{1}{4}}} \tag{3.3}$$

After the calculation using the y+ value as 1, the y_p value is approximated to be 0.0002 m, and the first layer mesh size in the rotating mesh zone is 0.0004 m height, 0.004 m width, as shown in figure 3.9. Using the similar method, the first layer mesh size for the stationary hub is 0.001 m height, 0.01 m width (substitute W with free stream velocity). The mesh size comparison is shown in figure 3.10. Both inflation layers used the default growth rate of 1.2.

Overall, the total mesh number is 11 million. The Minimum Orthogonal Quality = 7.61426e-02, and the Maximum Aspect Ratio = 5.27470e+01. The average Skewness = 0.21271, and the Average Orthogonal Quality = 0.78564.

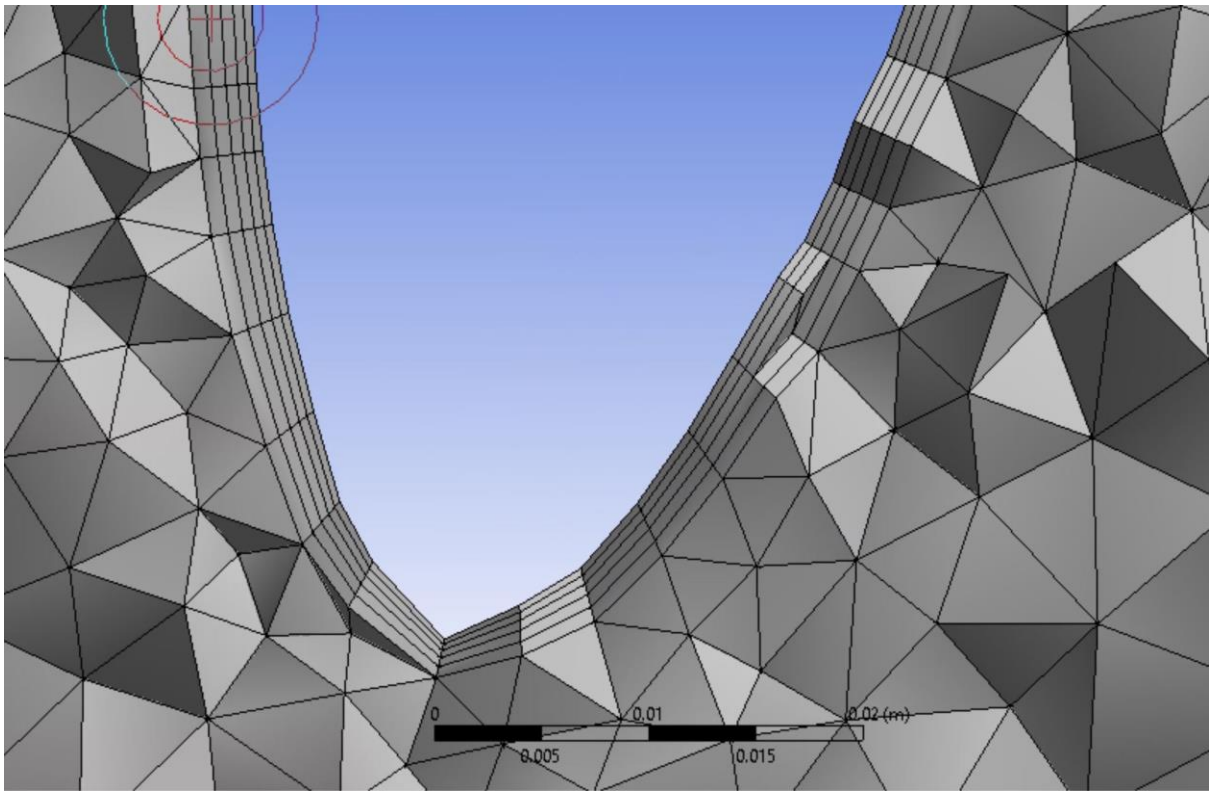

Figure 3.9 Inflation layer in the rotating mesh zone

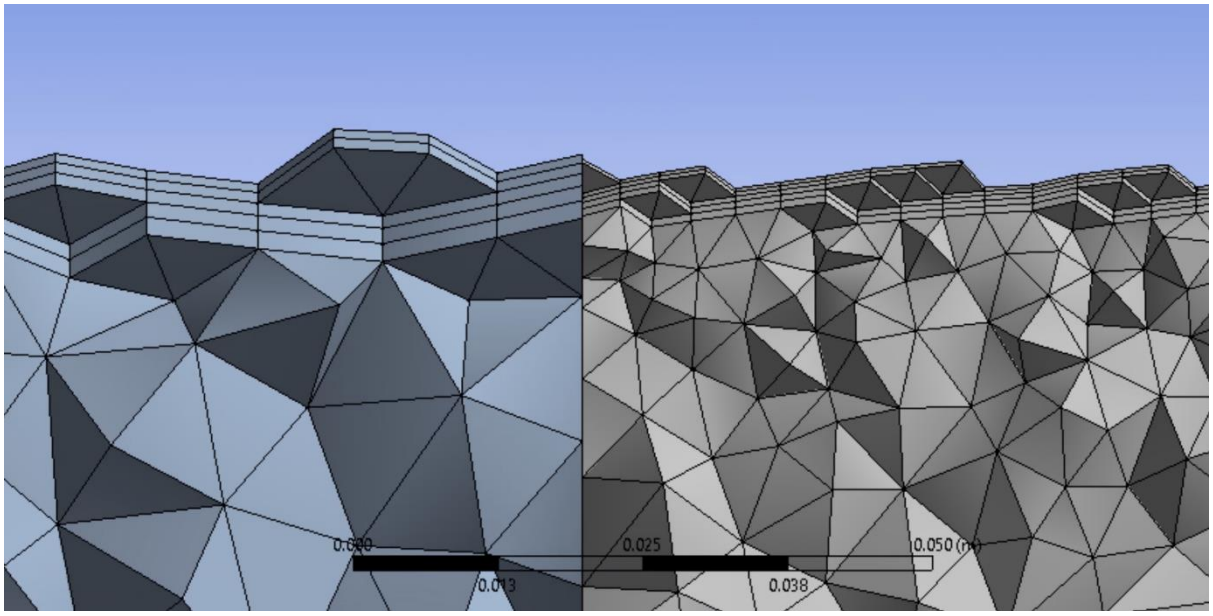

Figure 3.10 Inflation size comparison between rotating and stationary zones

3.3 Simulation Setups

This CFD study employs ANSYS Fluent 2020 R2 for CFD simulation. The simulated turbine working conditions are free stream velocity of 1.5 m/s and 35 rpm, which is consistent with the Schottel on-site test [6]. The boundary conditions are presented in the following figure:

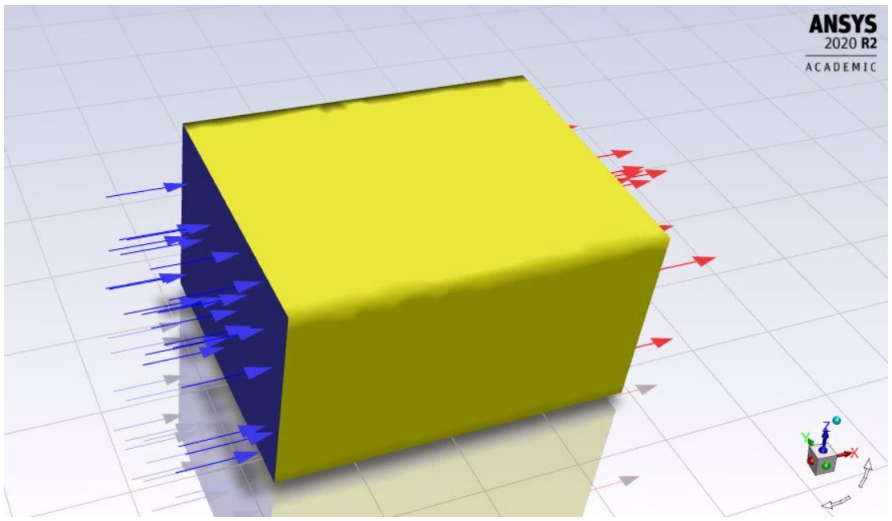

Figure 3.11. Fluent setup model

The blue arrow represents the inlet flow, the red arrow represents the outlet flow, and the yellow faces are set as symmetry which can simulate the unbounded water channel of ocean environment.

The converged simulations employed 13300 timesteps for a timestep size of 0.002s, and 6600 timesteps for a timestep size of 0.004s, which results in a flow time of around 26 seconds. Each timestep runs for 20 iterations unless the residuals converged. For 0.002 timestep size simulation, the converged residuals were set to be 1e-3 for quicker convergence and the residuals reached convergence less than 20 iterations. The later simulations set the residuals convergence to 1e-4 for more accurate results. The chosen flow time is the minimum simulation duration to make sure that the residuals, contour plots and torque values are all converged. The Owens Supercomputer from the Ohio Supercomputer Center has been used for the 11 million cells calculation. The simulation runs for 40 hours, using 2 nodes, 56 Intel Xeon E5-2680 (Broadwell) CPUs in total for parallel computing. The ANSYS Fluent 2020 R1 is the version that being used on the Owens for this study.

In addition to the residuals of the governing equations, the parameter being monitored during simulation is torque, and the rotating turbine parts are involved in the torque calculation:

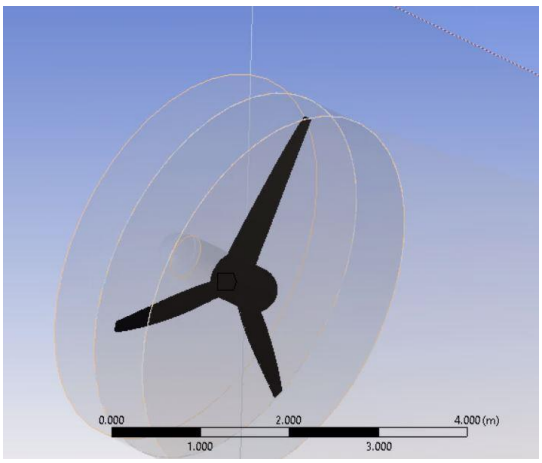

Figure 3.12 Rotational parts of the turbine

The torque value calculated is then converted to power to compare with the data gathered from on-site test, where ω is the angular velocity of the turbine (rpm) and T is the torque being recorded in FLUENT:

$$P = \omega T = \omega(\text{rpm}) \cdot \frac{2\pi}{60} T \tag{4}$$

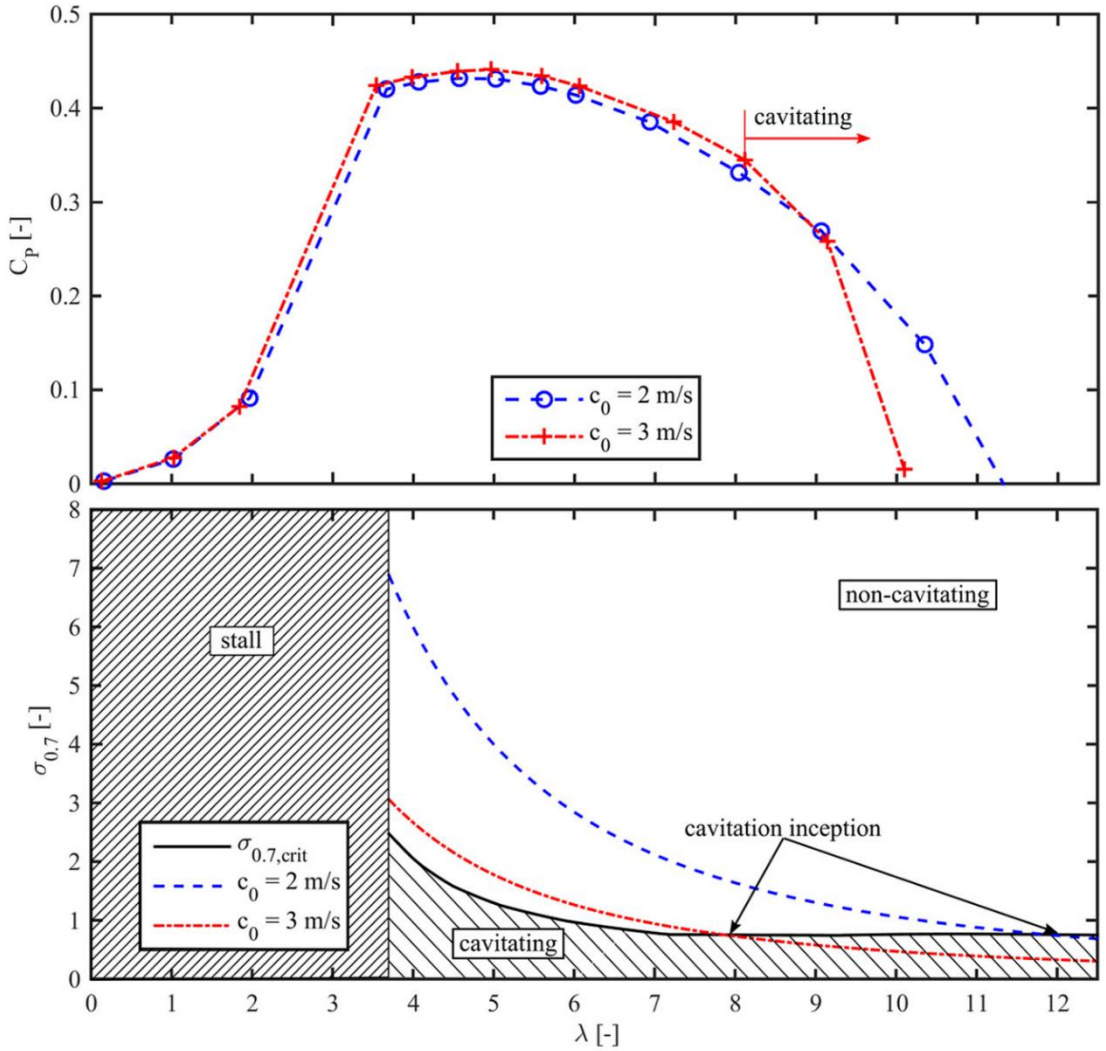

Figure 3.13 Tow test Power Coefficient Result [4]

According to a tow test done by Schottel [4], the optimal Tip Speed Ratio is around 5, shown in figure 3.13. Based on a flow velocity of 1.5 m/s, the rpm can be calculated to be 35:

$$\lambda = \frac{U_{tip}}{U_{flow}} \tag{5.1}$$

$$U_{tip} = r\,\omega \tag{5.2}$$

$$\omega = \frac{U_{flow} \cdot \lambda \cdot 60}{2\pi r} \approx 35(rpm) \tag{5.3}$$

$$\omega = \frac{\mathrm{U_{flow}}\lambda}{\mathrm{r}} = 3.665(\mathrm{rad/s}) \tag{5.4}$$

where U_flow is the freestream velocity, U_tip is the velocity of the blade tip, λ is Tip Speed Ratio, and r is the blade radius.

The flow field will be analyzed by taking 2 cuts through the domains and employing contour plots of a variety of flow variables The two planes used to show these 2D contour plots are given in the following. Figure 3.14 is the plane that represents the flow domain. It also vertically cuts through one blade and can be used for the analysis of the flow condition around the whole turbine geometry. Figure 3.15 is the plane that cuts through the 2/3 radius location of one turbine blade to show the flow field in the vicinity of the blade.

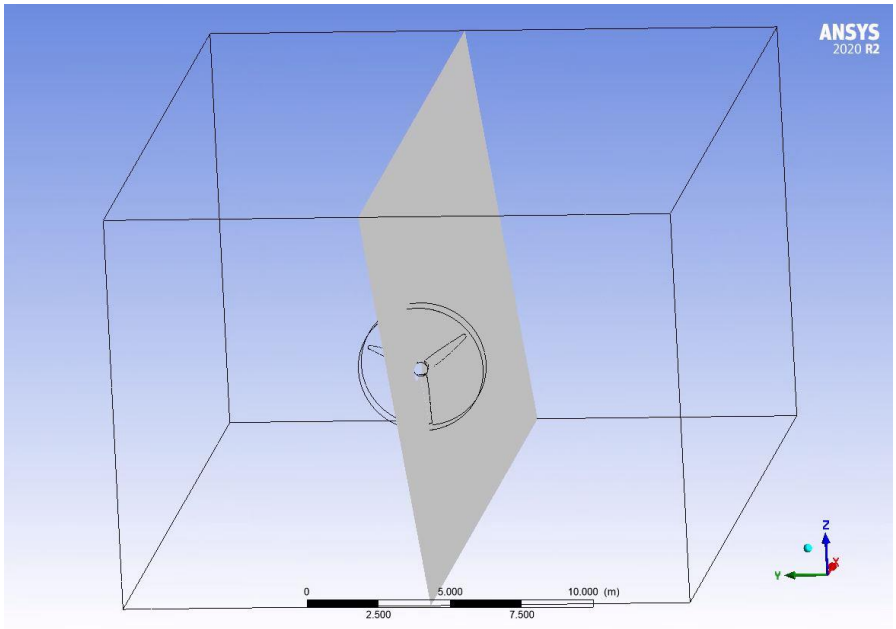

Figure 3.14 Vertical section view of one blade

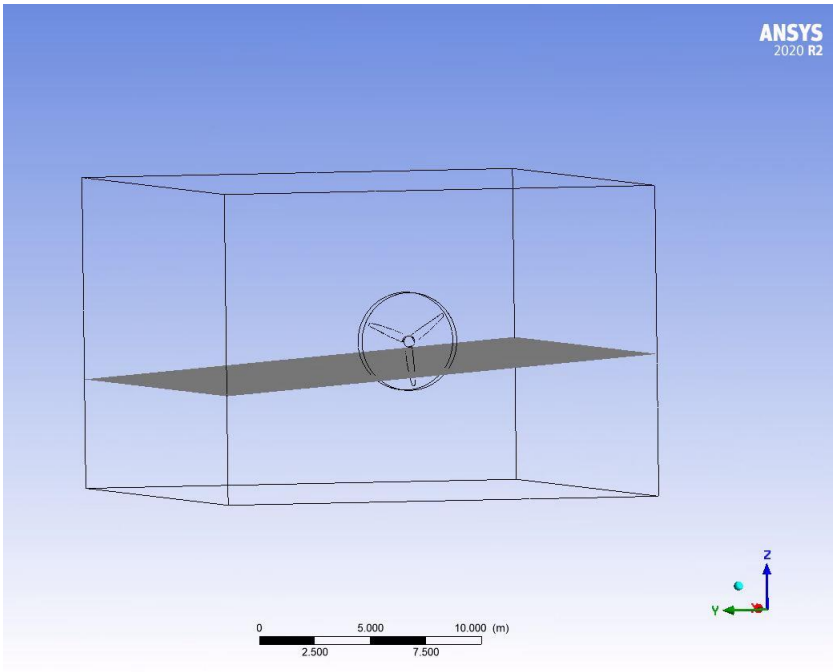

Figure 3.15 Horizontal section view

3.4 Convergence Study

Simulation Convergence

Besides the mesh size, timestep size and duration are essential to provide a converged solution for simulation as well. The initial timestep size is determined by the smallest mesh size at the 2/3 radius and the relative flow speed at the same location. The velocity is measured on the blade velocity contour plot.

$$V_{max} = 6.303 m/s \tag{6.1}$$

$$V_{Timestep} = 6.303 m/s \cdot 0.002 s = 1.26e-2 m \tag{6.2}$$

$$\#_{element} = \frac{1.26e-3}{4e-3} = 3 \tag{6.3}$$

At the fastest flow location, the flow passes three elements at one timestep, which is accurate enough for the 35 rpm, $u_{flow} = 1.5\ m/s$ conditions. Figure 3.16 is the velocity

contour of the horizontal blade section view, and the Vmax value is determined from the result. The velocity contour also showed that the result is resolved in the boundary layer.

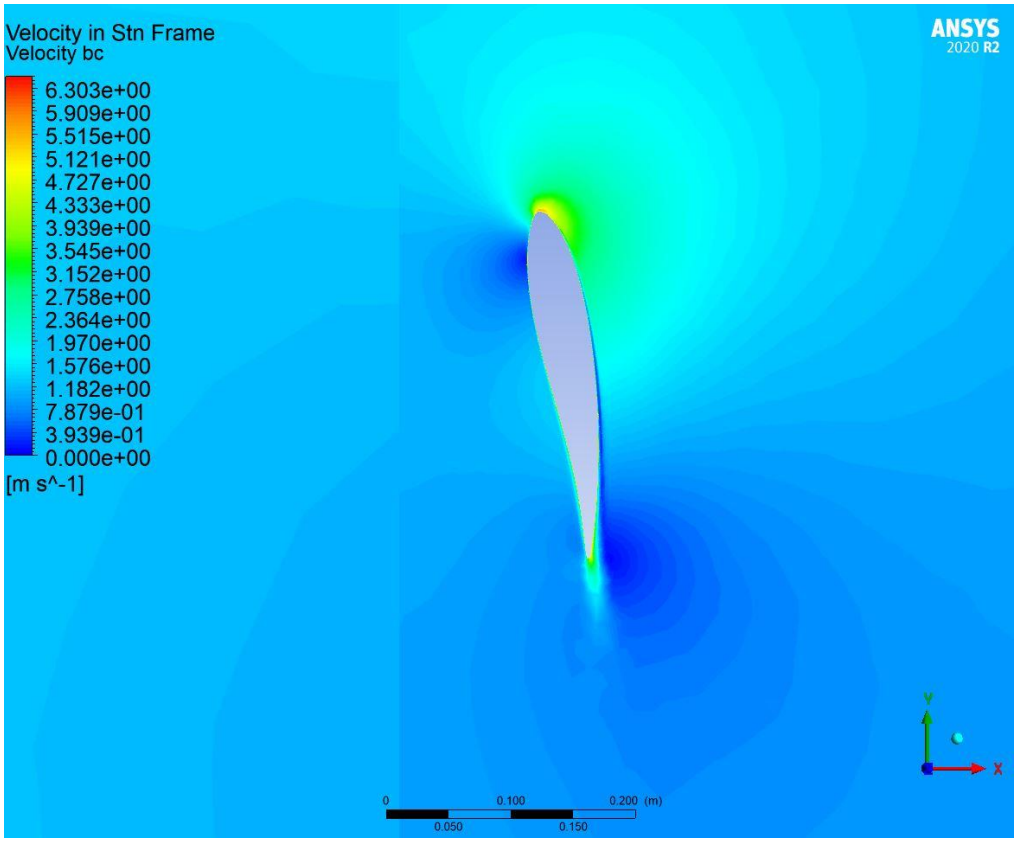

Figure 3.16 Velocity distribution around the 2/3 radius of blade

The duration of the simulation depends on the convergence of three results: velocity contour, residuals, and torque result. The initial convergence study is based on the case with a timestep size of 0.002s and 11 million cells. Figure 3.17 is the velocity field contour plot after 12300 iterations, which gives a flow time of 24.6 seconds. Figure 3.18 is the velocity field contour plot after 13300 iterations, which means a flow time of 26.6 seconds. The velocity distributions are almost identical, which means the solution is converged in terms of the velocity contour plot.

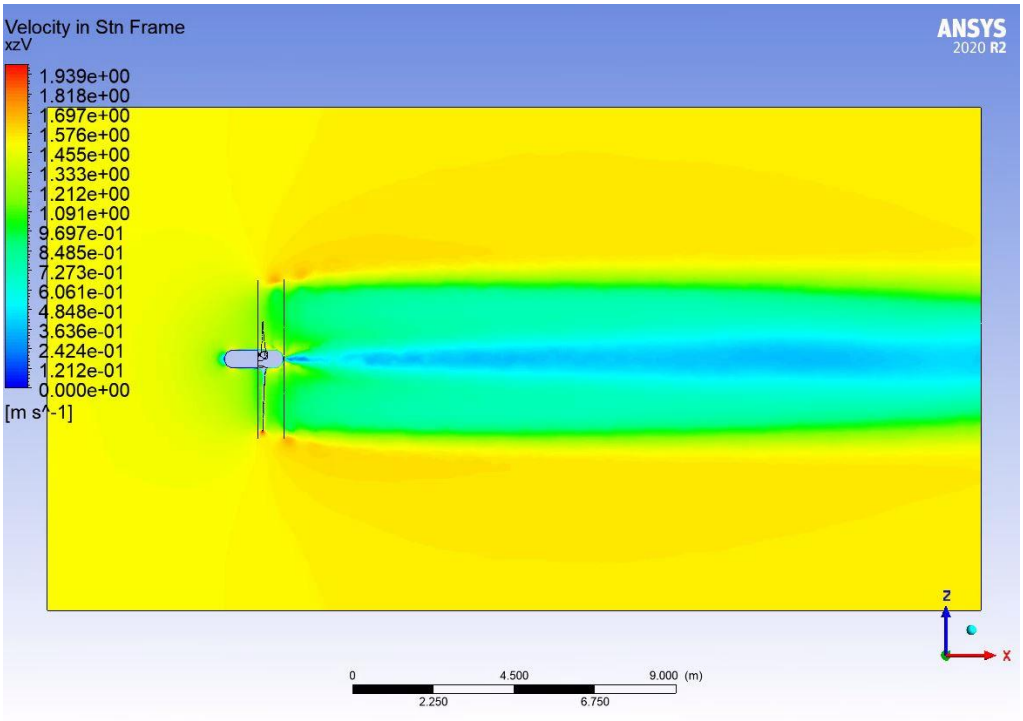

Figure 3.17 Timestep size =0.002s, flow time = 24.6s

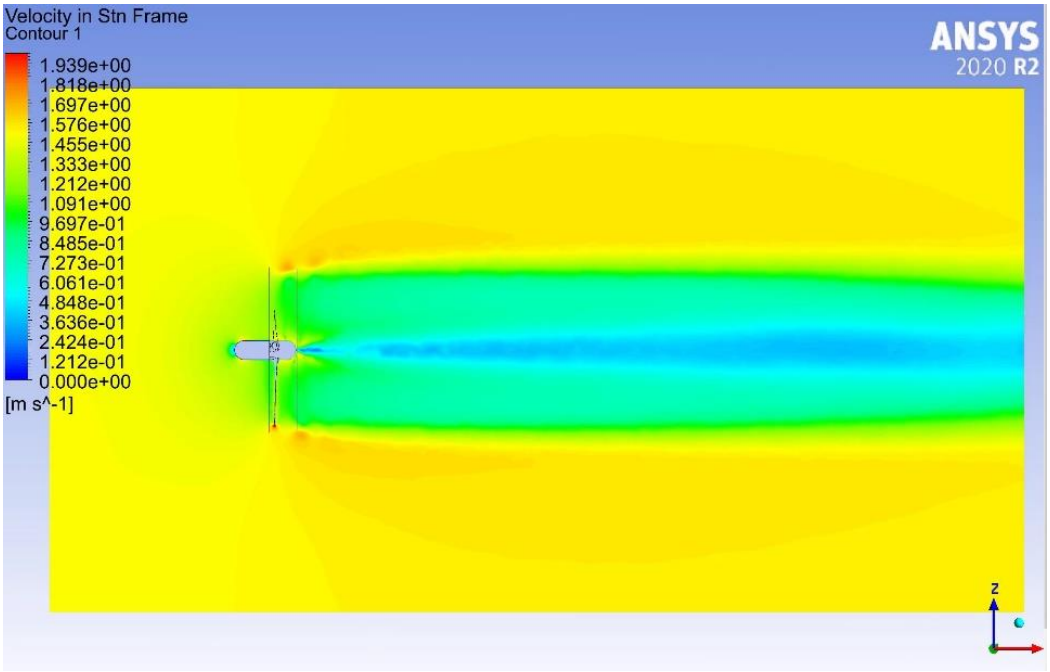

Figure 3.18 Timestep size = 0.002s, flow time = 26.6s

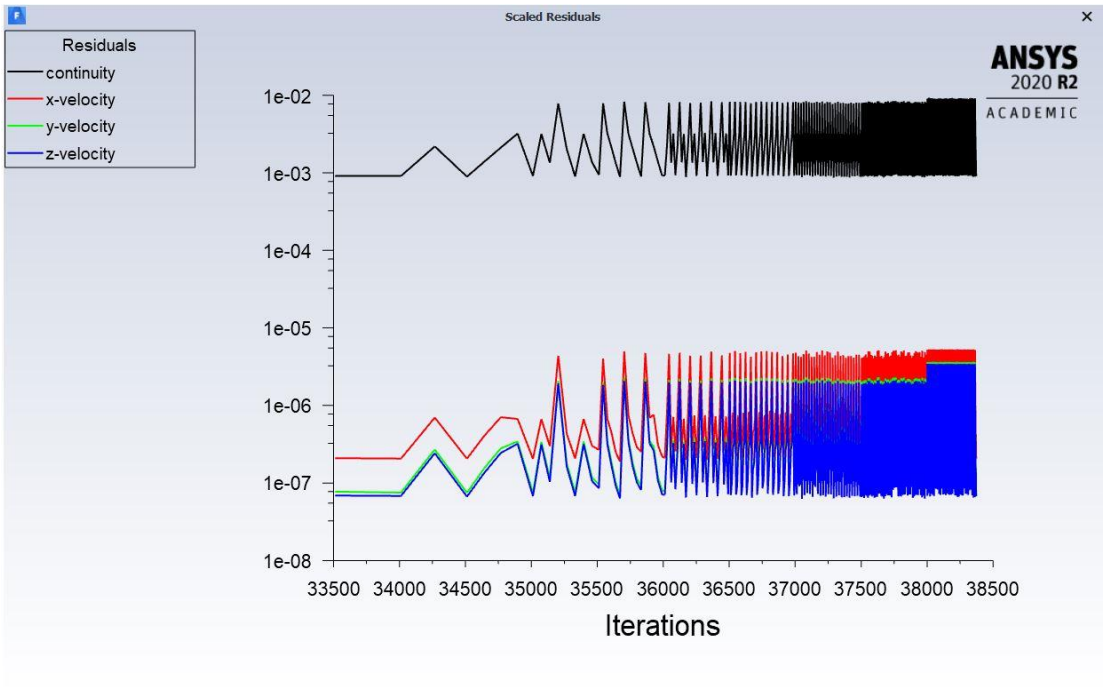

Figure 3.19 Residuals for timestep size =0.002s

The residual plot in figure 3.19 and the torque results in figure 3.20 both show that the flow field is converged at a flow time of 26s.

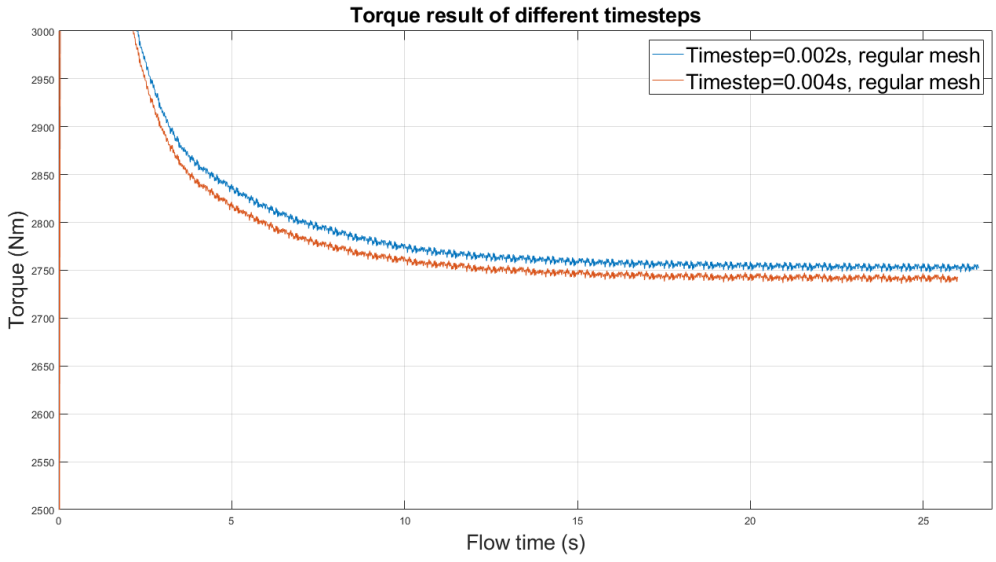

Figure 3.20 Torque plot of different timesteps

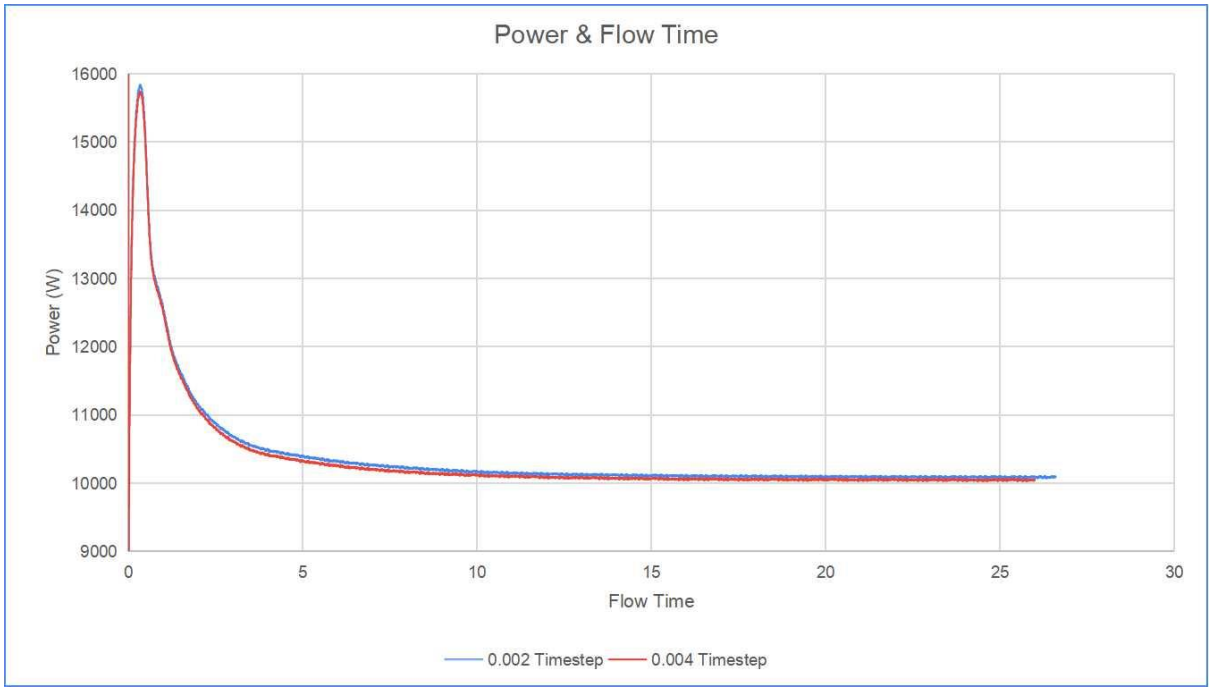

Figure 3.21 Simulated power output for different timesteps

The power outputs in figure 3.21 shows the converged power value to be 10 kW.

The red line in figure 3.20 and figure 3.21 are the results using a timestep size of 0.004s, which only takes 6600 iterations to reach a flow time of 26.4s. Both plot show that the 0.004s timestep gives a converged solution as well and the results are the same as 0.002s timestep size. Figure 3.22 is the velocity contour plot 0.004s timestep size and figure 3.23 is the residual plots for 0.004s timestep size. Both plots can show that the results are the same for 0.002s and 0.004s timestep size. For the purpose of saving computation time, the results in the following parts are based on the timestep size of 0.004s.

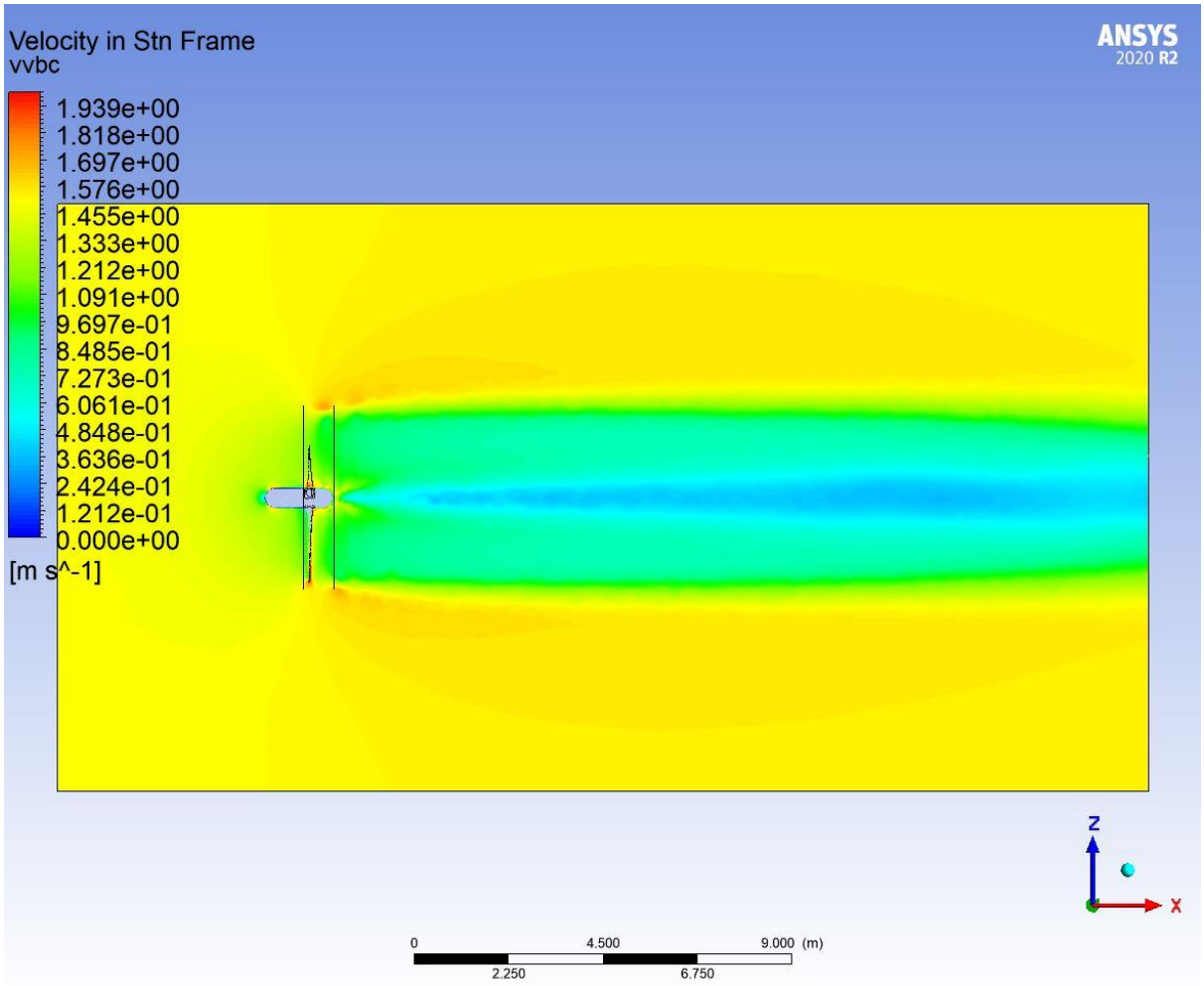

Figure 3.22 Velocity contour for timestep size of 0.004s, 26s flow time

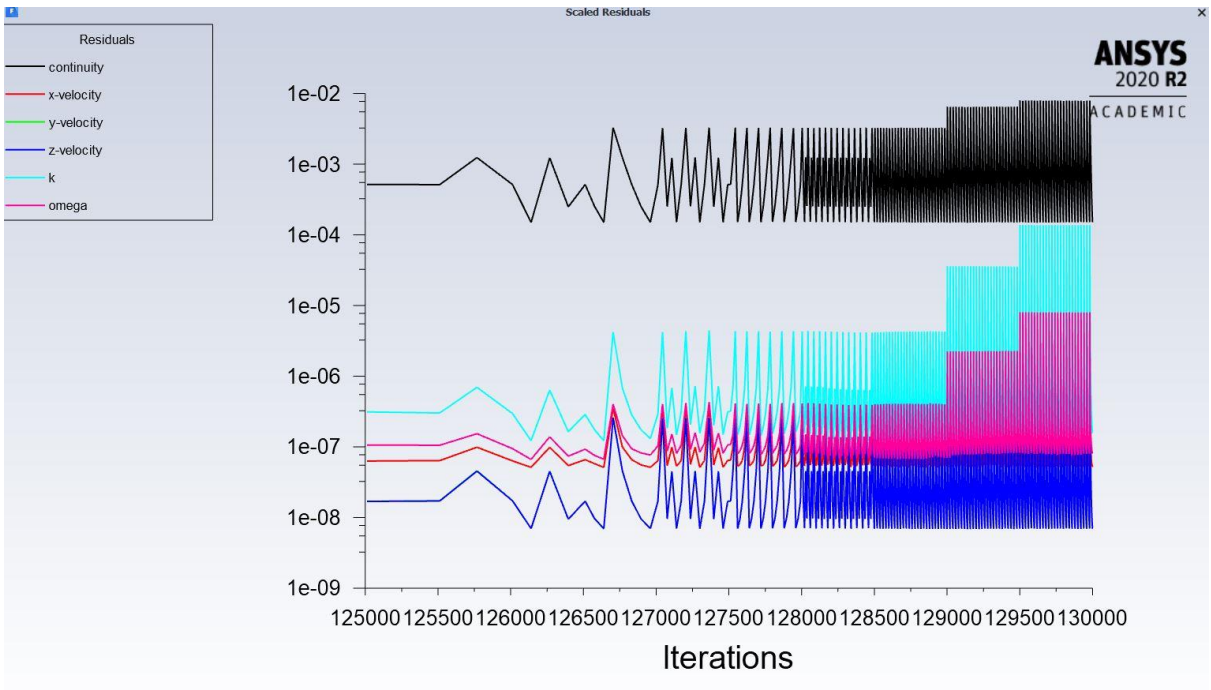

Figure 3.23 Residual plot for timestep size of 0.004s, 26s flow time

Grid Convergence

As part of a grid convergence study 3 different size grids have been compared, fine mesh, regular mesh, and coarse mesh. The coarse mesh is developed by expanding the size of the regular cells with a factor of 1.5, which results in a total mesh number of 5.2 million cells. The fine mesh reduced the regular cell size by a factor of 1.5 which leads to a total cell number of 24 million. The timestep size of the fine mesh simulation also reduced by 1.5 times, which gives a timestep size of 0.0025s. The following plots compare the three grids in a variety of convergence criteria: equation residuals, flow field and torque convergence.

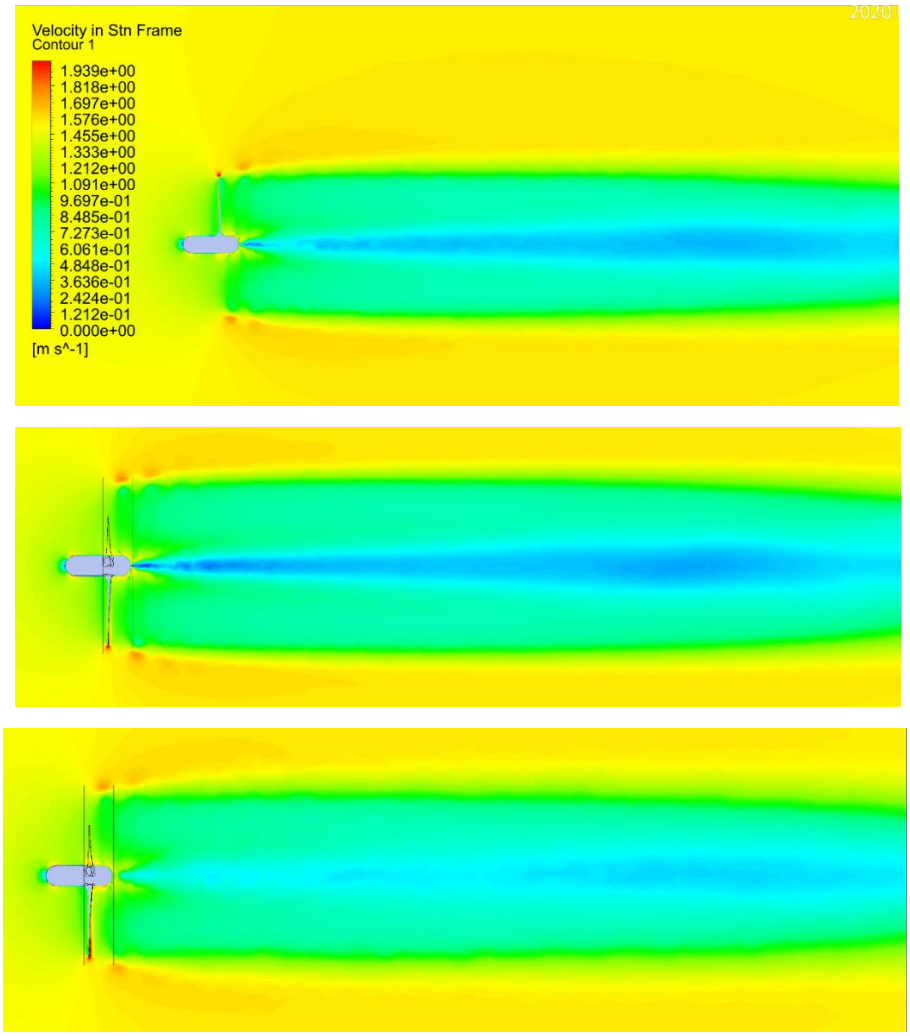

Figure 3.24 (From top to bottom) Flow field velocity contour of 11 million, 24 million, and 5.2 million cells

The velocity contour in the wake regions of 5.2 million cells contains less details in the velocity distribution of the turbulences, which means 5.2 million cells are not sufficient for the further analysis of the wake flow. The velocity contour between 11 million cells and 24 million cells are almost identical.

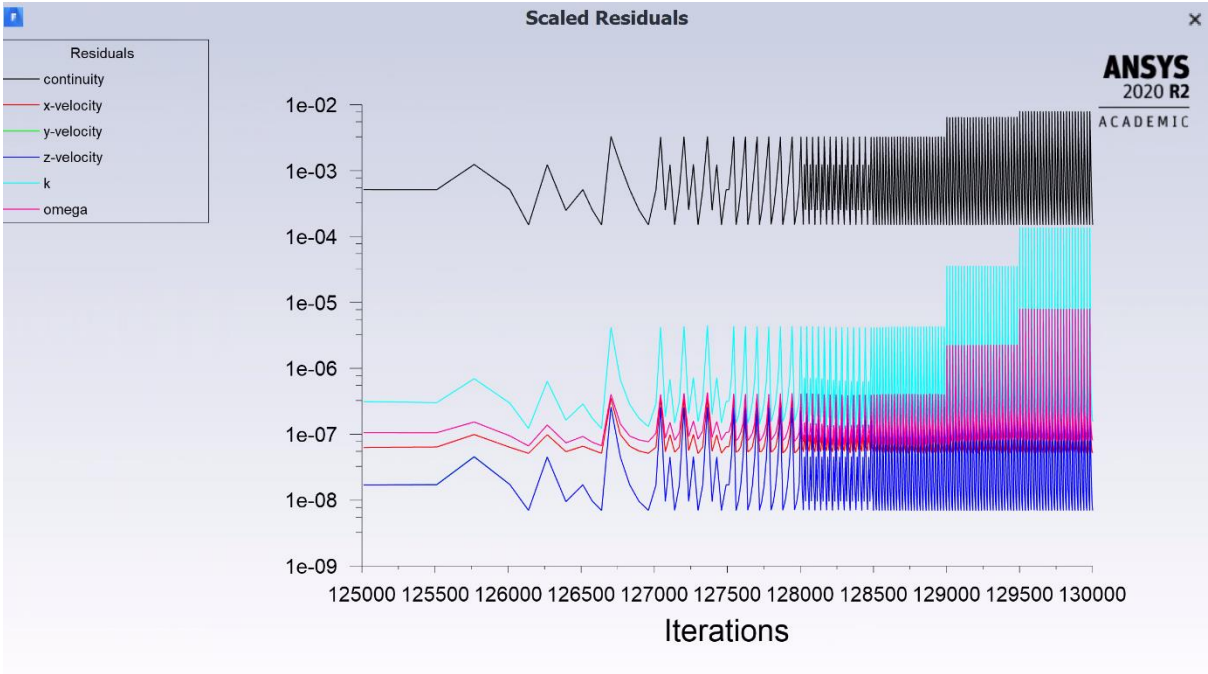

Figure 3.25 Residual plot for 5.2 million cells

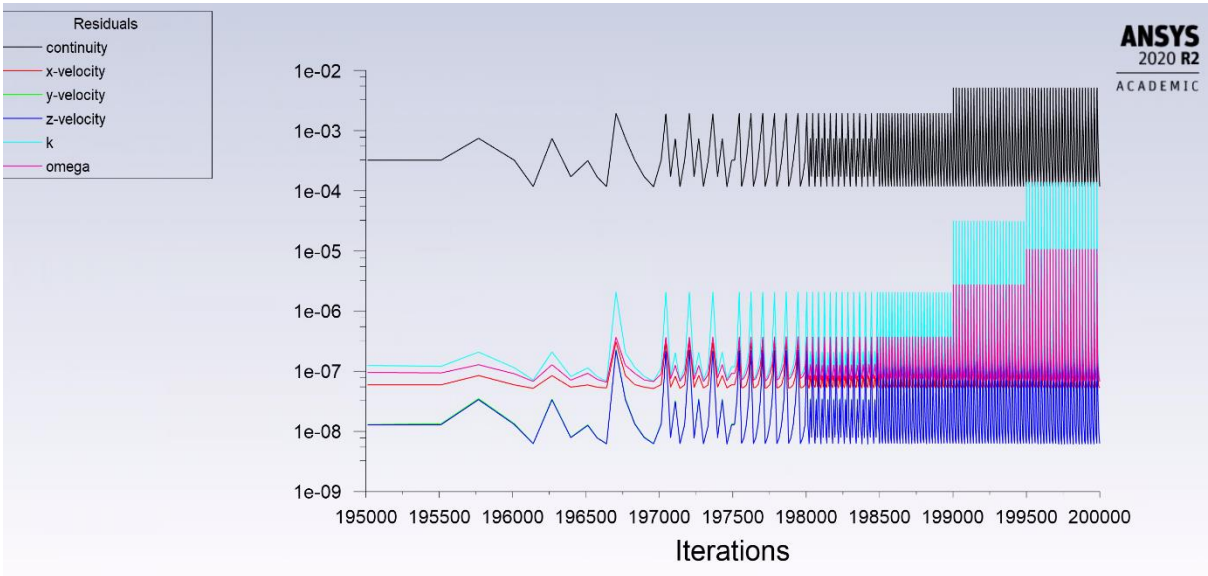

Figure 3.26 Residual plot for 24 million cells

Combining with the residual plots in figure 3.23, 3.25 and 3.36, the simulation of three different mesh sizes all converged despite the different results. The continuity was high at the beginning of each timestep and falls to acceptable range after 20 iterations.

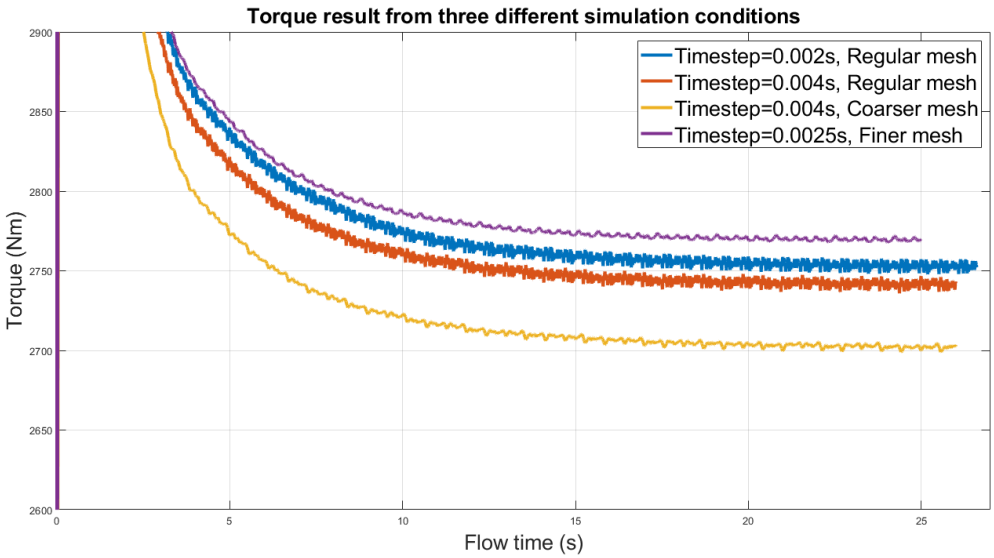

Figure 3.27 Torque comparison between 5.2 million cells (Yellow), 11 million cells (Red) and 24 million cells (Purple)

The torque result of 5.2 million cells case is significantly smaller than the 11 million cells case while the torque result of 24 million cells is slightly larger than the regular mesh result. Table 1 shows the torque comparison and the percentage differences. The result between 11 and 24 million cells are less than 1% which means the torque result of 11 million cells is acceptable.

Number of Cells (million)	Torque (Nm)	% Torque differece compare to 11 million cell mesh
11	2742.3	-
5.2	2703.5	1.42%
24	2768.8	0.97%

Table 1. Comparison between number of cells and torque result

Overall, the 5.2 million cells will affect the simulation results and 24 million cells takes too much computation time. and the minimum cell number is 11 million.

Chapter 4. Results Analysis

4.1 Flow Field Analysis

The simulations for four different rotational velocities have been performed with a flow velocity of 1.5 m/s, 11 million cells, 0.004s timestep size, and 26.4s flow time.

Figure 4.1 presents the velocity contour plot around a turbine blade at the 2/3 radius when the rotational velocity is 15rpm, which shows the blades are in stall condition due to the small relative rotational velocity compared to the flow speed. As a result, the further flow domain analysis does not include this low rotational velocity simulation case.

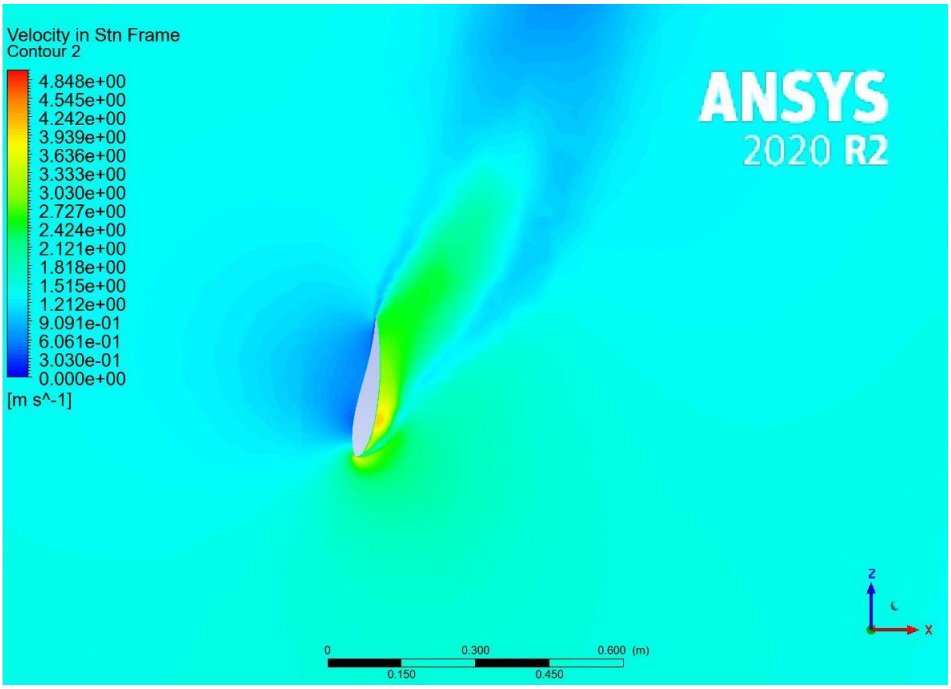

Figure 4.1 Velocity around blade when rpm = 15

Figure 4.2 shows the velocity magnitude across the domain. All views presented pass through the origin and the wake region is a 3D cylinder as shown in figure 4.3. The results indicate that when the rotational velocity is lower, the turbine resistance posed to the flow is smaller, which leaves a wake region with higher average velocity. It is further noted that the position

of the lowest velocity region (dark blue) shifts further downstream along the x axis with the increase of the rotational velocity.

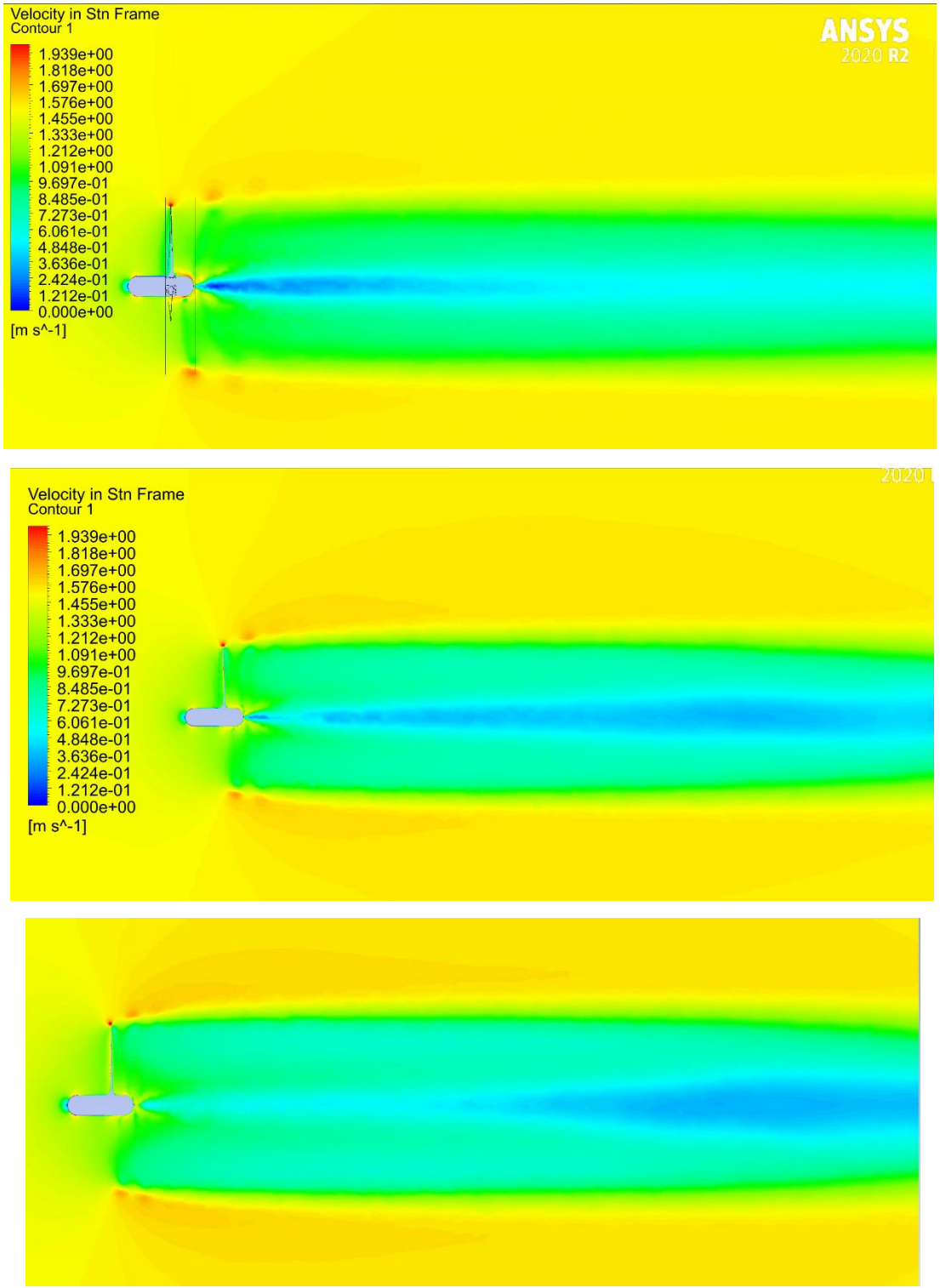

Figure 4.2 Flow field velocity contour plot for 25rpm, 35rpm, 45rpm (From top to bottom)

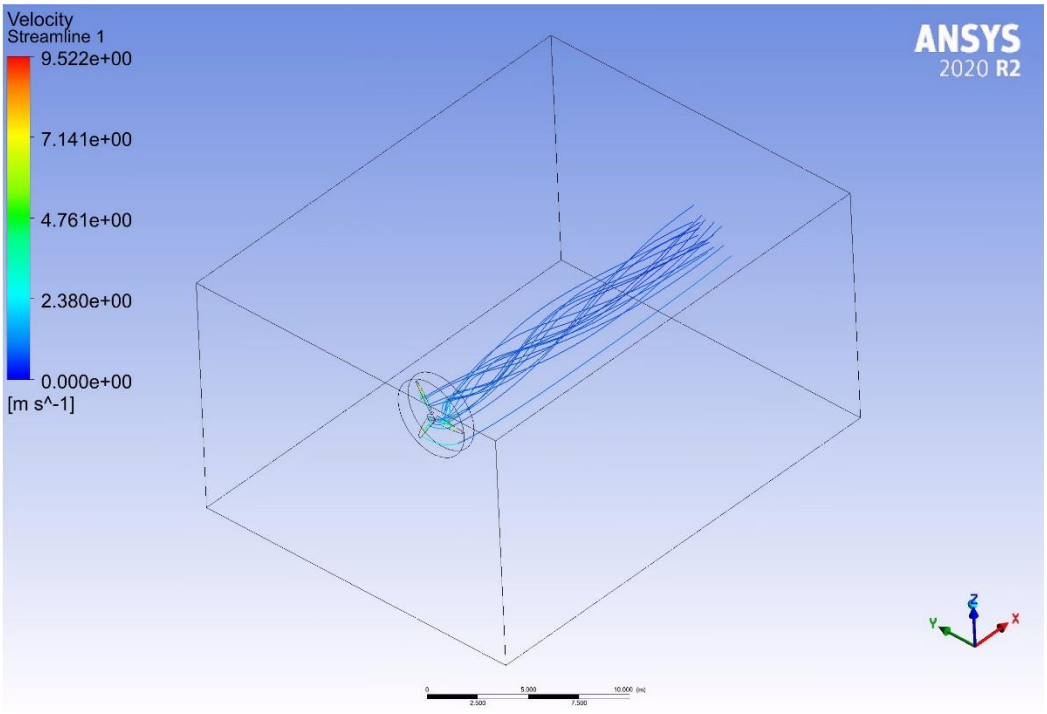

Figure 4.3 Wake Domain

Figure 4.4 shows the velocity contours around the blade section at 2/3 blade span. The maximum velocity in all three cases is observed at the tip of the blade. Flow separation is the most apparent when for a rotational velocity of 25rpm, which operates close to stall conditions.

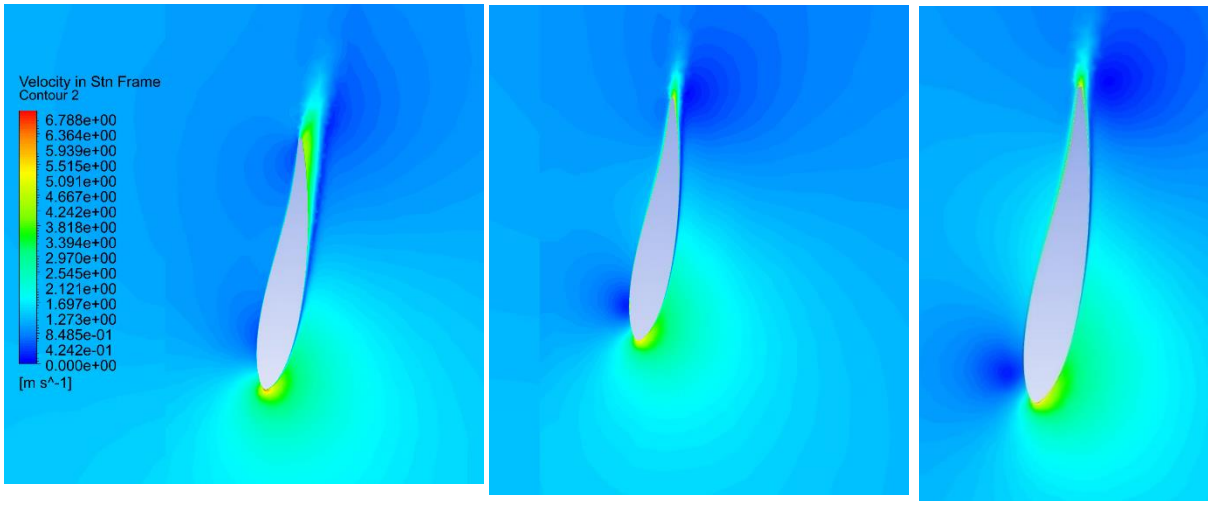

Figure 4.4 Velocity at the 2/3 blade span. 25rpm 35rpm 45rpm

Figure 4.5 is the pressure distribution around the turbine. The pressure distributions are similar for three rotational velocities, high pressure region in front of the blades and low-pressure region after the blades.

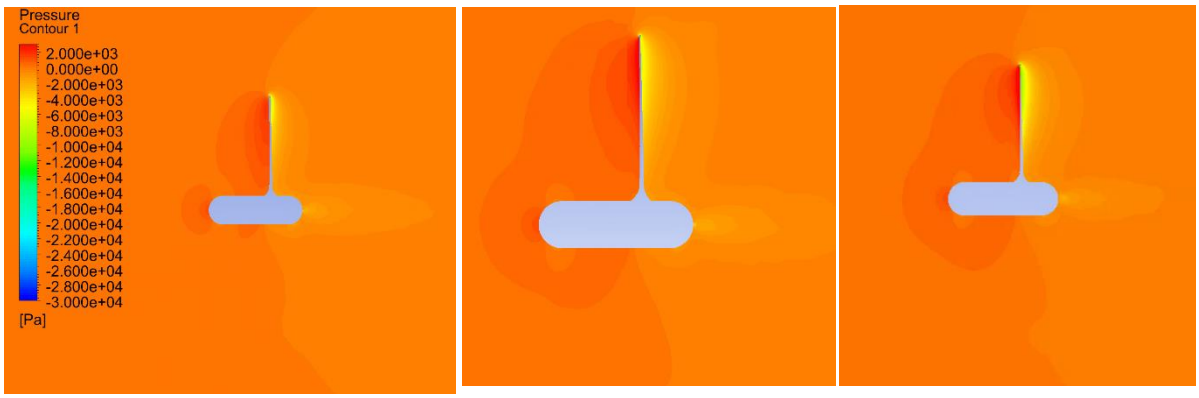

Figure 4.5 Pressure around turbine 25rpm | 35rpm | 45rpm

Figure 4.6 presents the pressure contours around the blade section view at 2/3 of blade span. The pressure range on the legend is broader than figure 4.5. The pressure distributions on the leading edge are as expected, with a stagnation pressure region shown in red and a low-pressure region on the suction side of the airfoil. Looking at the trends by varying the rotational velocity, one can observe an increase in stagnation pressure as the rotational velocity increases.

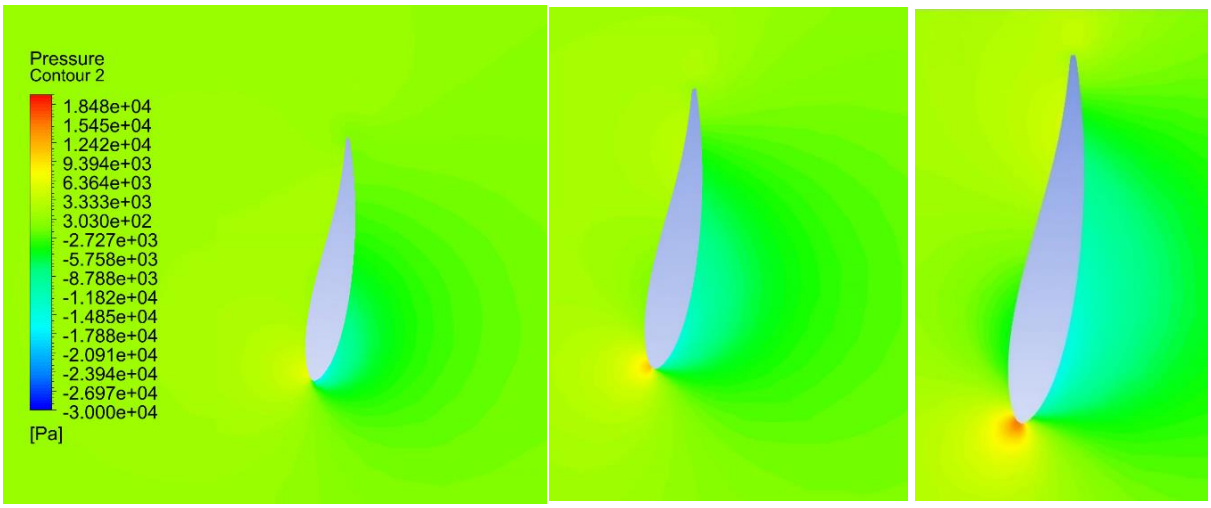

Figure 4.6 Pressure at 2/3 blade span 25rpm | 35rpm | 45rpm

The velocity distribution along a line parallel to the x axis (and thus the main flow velocity) is further analyzed to better understand the turbulent flow dissipation after the rotating blades. The end points of the chosen line are (-6, -1.333, 0) and (20, -1.333, 0), where 1.333 means the 2/3 span of the blade. The top view of the line (from +Z direction) is shown in figure 4.7.

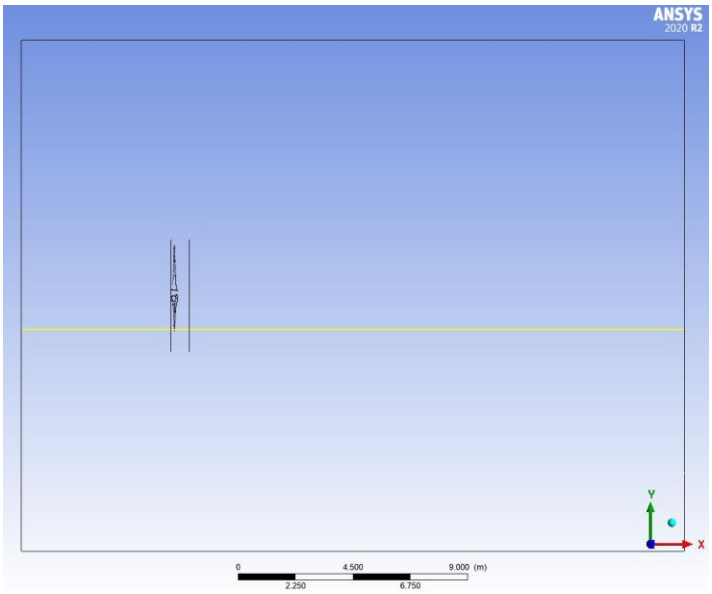

Figure 4.7 Record line position

The velocity distribution is shown in Figure 4.8, using 100 sample points along the line.

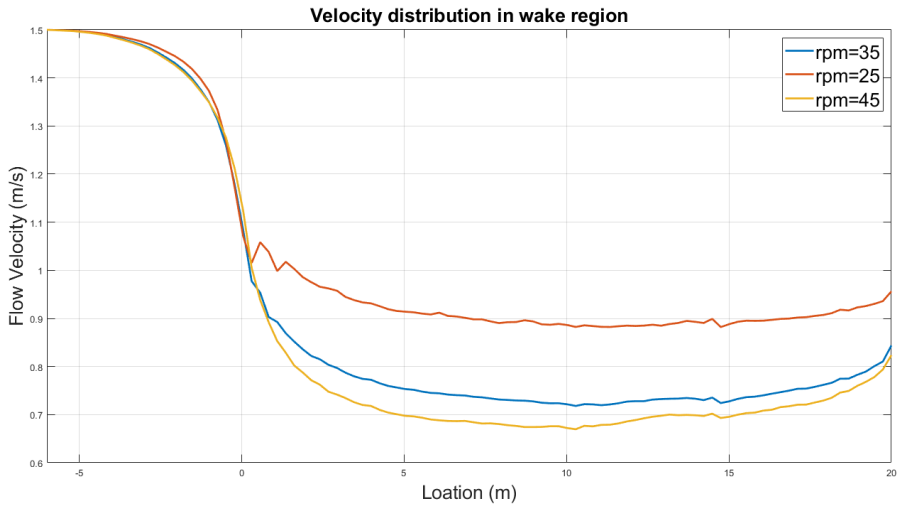

Figure 4.8 Velocity distribution

The result shows that the wake velocity is larger for lower rotational velocities, which confirms that the axial thrust exerted at higher rpm is increased, thereby reducing velocities in the wake. The wake dissipation is also clearly visible in a recovery of the velocity starting at about 10m downstream of the rotor.

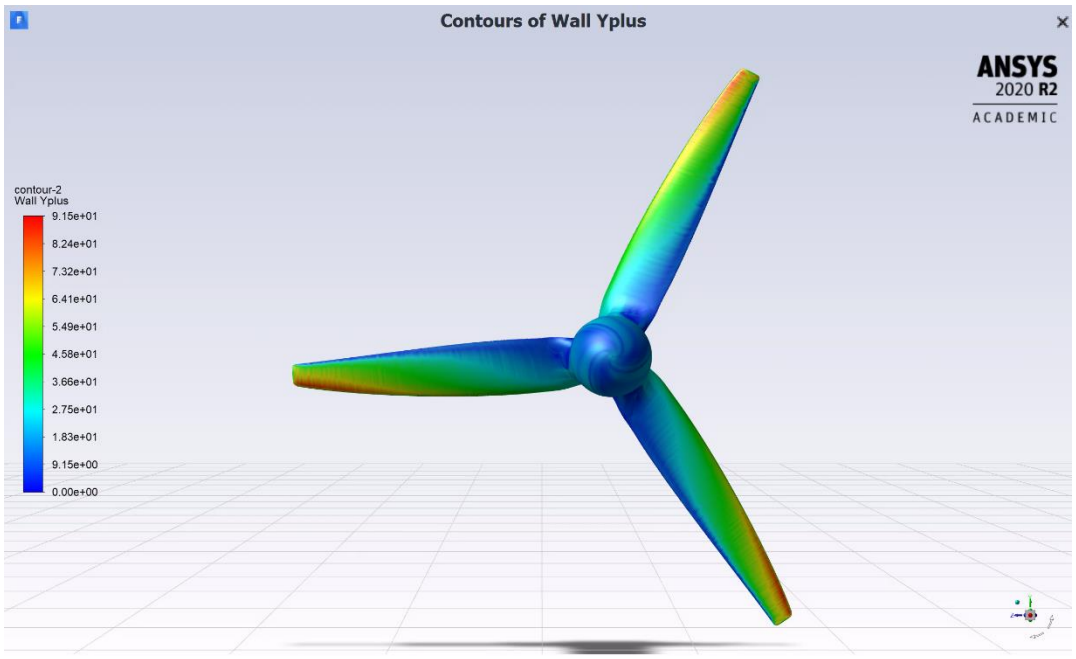

Figure 4.9 Wall Y+ contour on the turbine

The wall Y+ contour is plotted as figure 4.9, which shows that wall Y+ increases with the flow velocity pass the surface. The maximum Y+ value is at the tip of the leading edge. The observed Y+ value on the rotor is between 0 and 100.

For the 25rpm rotational speed is also analyzed for wake dissipation. Figure 4.10 shows the velocity data sampling lines at 1 to 5 diameter length along the x axis, and the velocity profiles in the wake region are shown in figure 4.11. It is noted that the velocity change ratio is largest at 1 diameter length and decreases along the increase of diameter length.

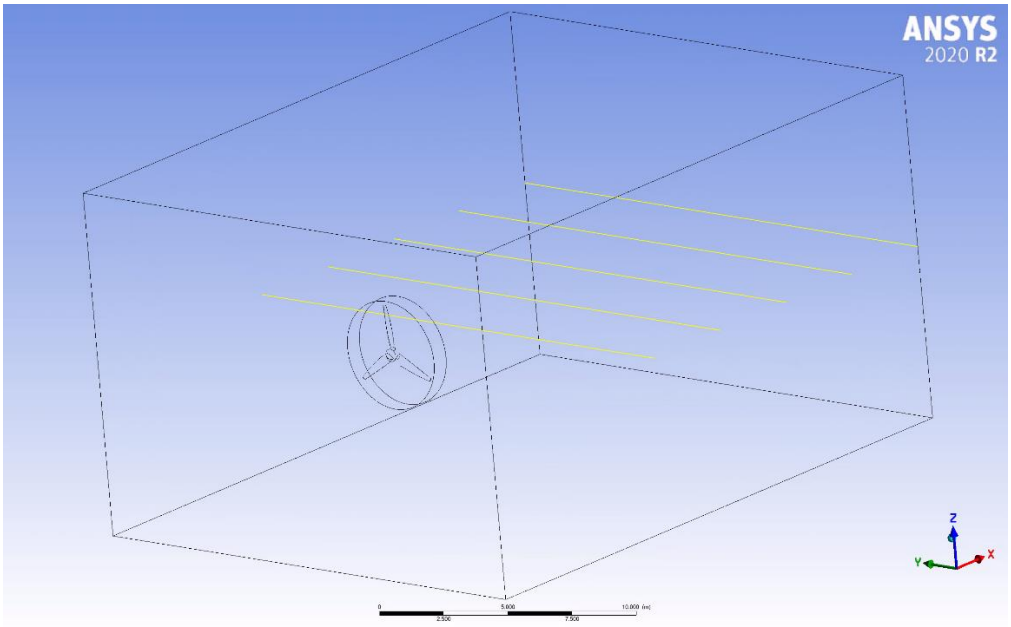

Figure 4.10 Velocity sampling location

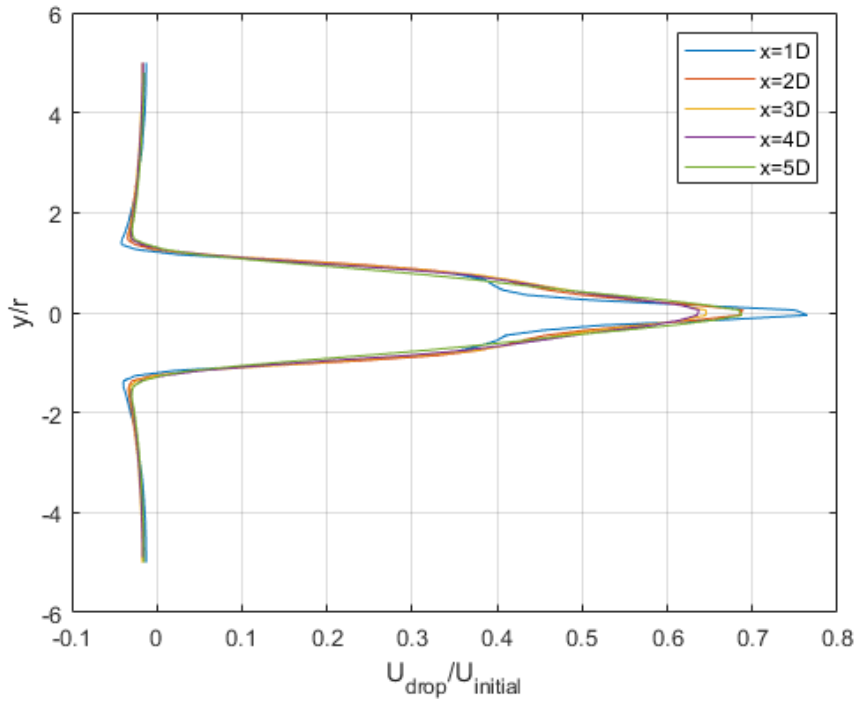

Figure 4.11 Velocity profiles of different diameter length

The equation of the velocity ratio is calculated as:

$$U_{Ratio} = \frac{U - U_{\text{initial}}}{U_{\text{initial}}} \tag{7}$$

Where $U_{initial}$ is the 1.5 m/s flow speed.

4.2 Performance Analysis for Different Rotational Speed

The extracted power and torque values are listed in Table 2. While the case of the very low rotational velocity of 15rpm was neglected in the flow domain analysis, it is included in the performance analysis.

RPM	TSR	Torque (NM)	Power (kW)	Power Coefficient
15	2.094395102	1235.2	1.94	0.091664811
25	3.490658504	3160.1	8.27	0.390917638
35	4.886921906	2742.3	10.05	0.474927633
45	6.283185307	2082.7	9.81	0.463749722

Table 2 Power and Torque values

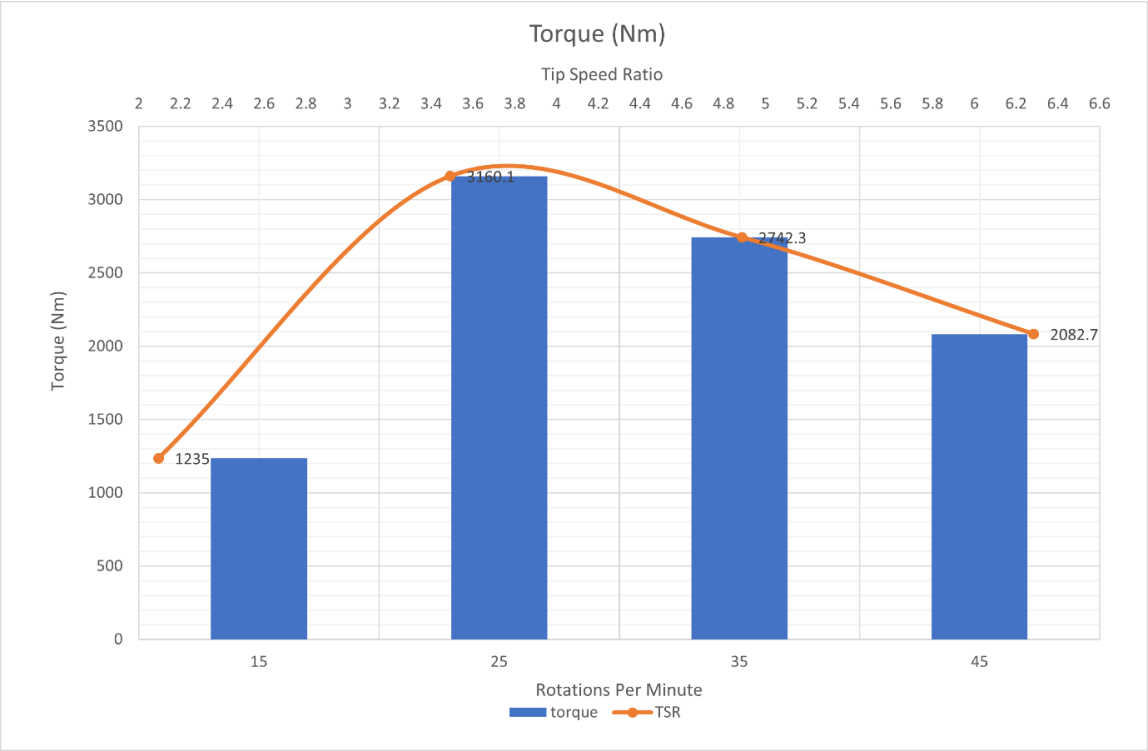

Figure 4.12 Torque at different rotational velocities and TSR

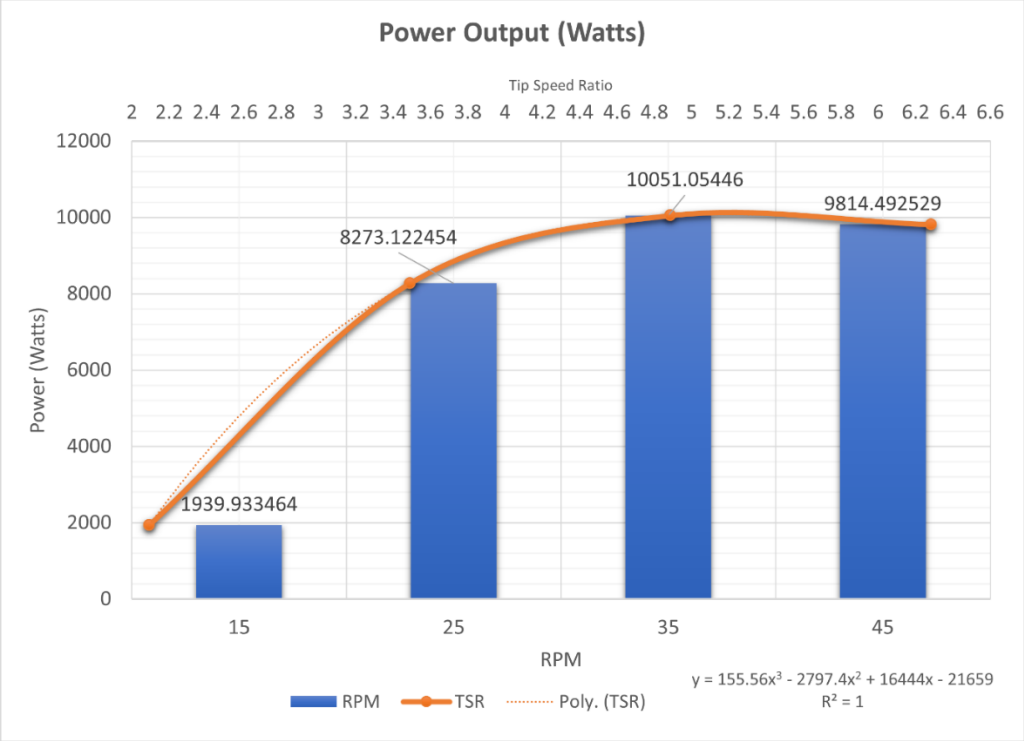

Figure 4.13 Power at different RPM and TSR

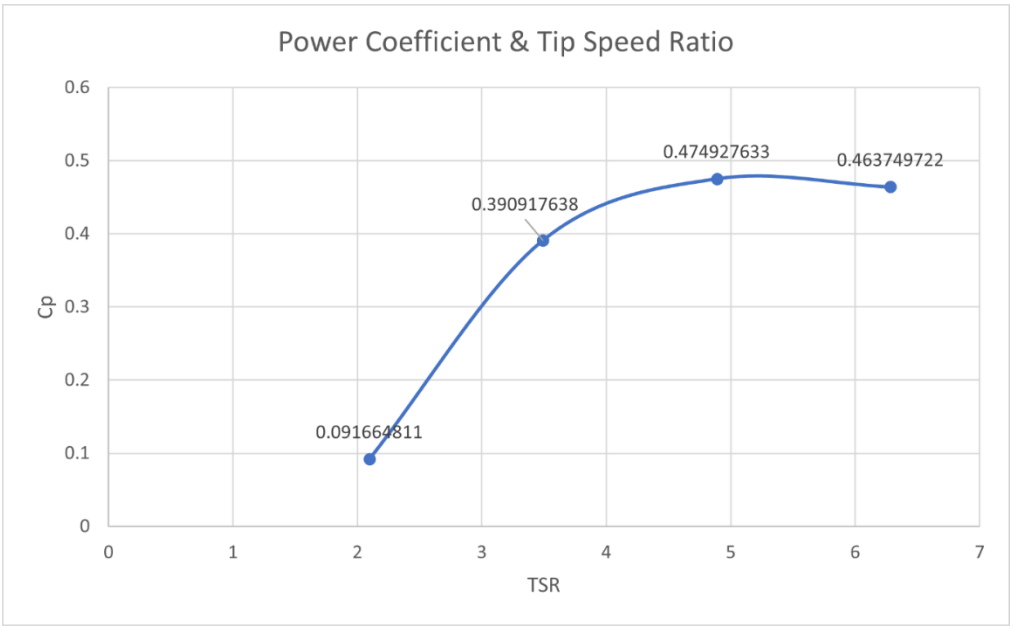

Figure 4.14 Simulated Power Coefficient

For a flow speed of 1.5 m/s. the maximum torque is estimated around the 25rpm rotational speed while the maximum power generated is estimated around 35rpm. The maximum power coefficient is estimated around a tip speed ratio (TSR) of 5.

4.3 Comparison to Experimental Results

The turbine manufacturer Schottel performed field measurements of the turbine in 2015 in tidal flows. The device was mounted on a floating moored barge. Testing was conducted over 48 days, for 288 h, during flood tides in daylight hours [6]. The converged electrical power value was measured to be 10 kW for 1.5m/s flow speed. Figure 4.15 shows all the electrical power output data gathered and figure 4.16 shows the mean electrical output for each tested velocity.

In figure 4.16, a red cross is marked to illustrate the simulated hydropower data. The simulation result shows a higher power output than the mean of the measurements. This is to be expected since the simulation only captures the hydrodynamic power. Mechanical losses from the turbine as well as the loss from the electrical generator are not included. Further, the measurements were conducted in turbulent flow which can further impact the performance.

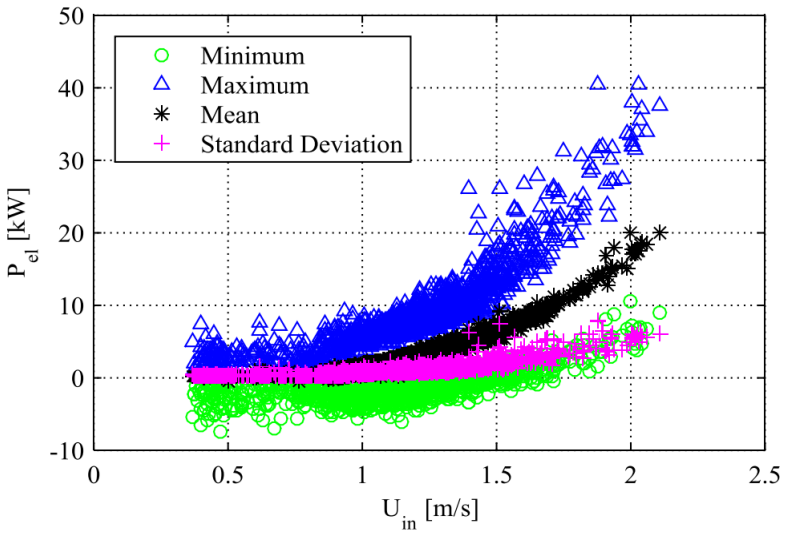

Figure 4.15 Power output data on site [6]

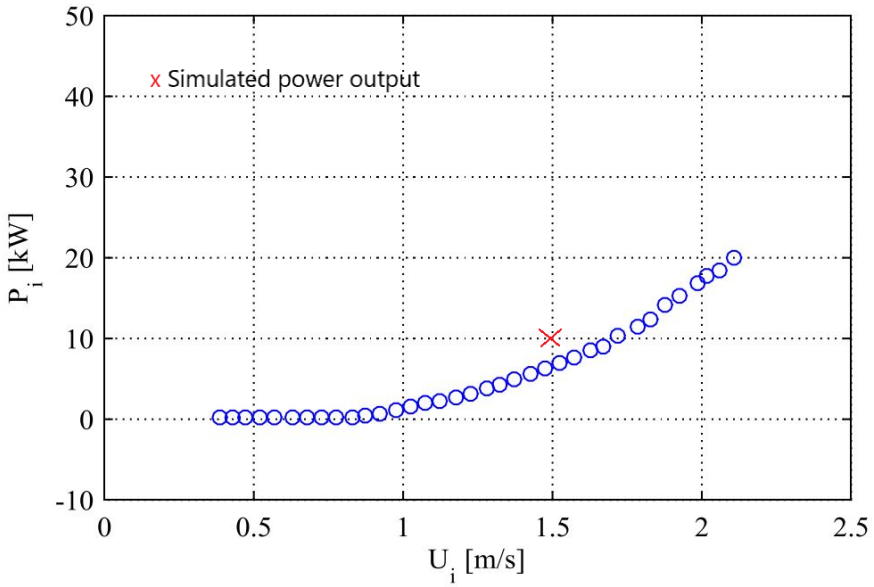

Figure 4.16 Mean power output data [6]

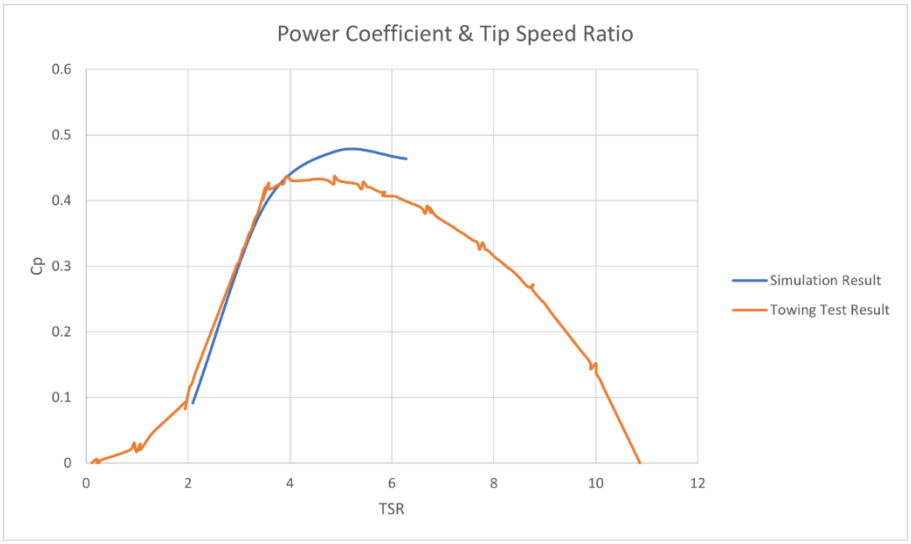

Figure 4.17 Power Coefficient Comparison between Simulation and Towing Test

Figure 4.17 is the comparison between simulated power coefficient and the pressure coefficient gathered from the towing test of 1:8 scale model. Based on the simulated data, maximum power is generated when TSR is 4.887. The trendline indicates that larger power may be found when TSR is between 4.8 and 6. The towing test data shows the same trend with different values on the power coefficient. Further simulation needs to be done at higher Tip Speed Ratio.

Chapter 5. Conclusion and Future works

The research started with a 3D model of SIT turbine, then the sliding mesh method was applied, and simulations of different rotational speeds were performed until the results converged. The convergence study included the simulation convergence and grid convergence to validate the simulation setups. Finally, the simulated results were compared to the experimental data gathered by Schottel, which validated the simulation when flow speed is 1.5m/s considering the possible loss factors.

The simulation can be further validated by employing different flow speeds and higher rotational speeds to have a more detailed comparison with the filed measurement data and the towing test data. The final goal of this research is to pave for the possibility of simulations involving a change of the turbine geometry, such as adding a duct for the turbine, and a further examination of its performance. This can be done after further validations are complete to ensure the simulation results will match the actual turbine performance.

References

[1] British Petroleum. 2019. *BP Statistical Review of World Energy*, 68th Edition.

[2] Ana Brito e M, Henry J. 2019. An overview of ocean energy activity in 2019. The Executive Committee of Ocean Energy Systems. Available from https://www.ocean-energy-systems.org/about-us/annual-report/

[3] Ocean Energy Systems. 2017. OES Vision for International Deployment of Ocean Energy. Ocean Energy Systems and International Energy Agency. Available from https://www.ocean-energy-systems.org/news/oes-vision-for-international-deploymentof-ocean-energy/

[4] N. Kaufmann, T. H. Carolus, and R. Starzmann, "An enhanced and validated performance and cavitation prediction model for horizontal axis tidal turbines," *Int. J. Mar. Energy*, vol. 19, pp. 145–163, 2017, doi: 10.1016/j.ijome.2017.07.003.

[5] N. Kaufmann, T. Carolus, and R. Starzmann, "Turbines for modular tidal current energy converters," *Renew. Energy*, vol. 142, pp. 451–460, 2019, doi: 10.1016/j.renene.2019.04.120.

[6] P. Jeffcoate, R. Starzmann, B. Elsaesser, S. Scholl, and S. Bischoff, "Field measurements of a full scale tidal turbine," *Int. J. Mar. Energy*, vol. 12, pp. 3–20, 2015, doi: 10.1016/j.ijome.2015.04.002.

[7] "SIT Instream Turbine," *SIT INSTREAM TURBINE - SCHOTTEL Industries*. [Online]. Available: https://www.schottel-industries.de/en/schottel-industries-gmbh/schottel-hydro-gmbh/sit-instream-turbine

[8] Kajishima, T., Taira, K. *Computational Fluid Dynamics*. Switzerland: Springer, 2017

[9] ANSYS,Inc. *ANSYS Fluent Theory Guide* 14th Release. Canonsburg, PA: ANSYS, 2011

[10] ANSYS,Inc. *ANSYS Fluent Tutorial Guide* 18th Release. Canonsburg, PA: ANSYS, 2017

[11] B. R. Munson, *Fundamentals of fluid mechanics*. Hoboken, N.J: Wiley, 2013.

Appendix

Bash file for operations on OSC

```
#!/bin/bash
#SBATCH --job-name=parallel_fluent
#SBATCH --time=10:00:00
#SBATCH --nodes=2 --ntasks-per-node=28
#SBATCH -L ansys@osc:1,ansyspar@osc:40
#SBATCH -A PAA0023

set echo on
hostname
#
# The following lines set up the FLUENT environment
#
module load ansys
#
# Create the config file for socket communication library
#
# Create list of nodes to launch job on
rm -f pnodes
cat  $PBS_NODEFILE | sort > pnodes
export ncpus=`cat pnodes | wc -l`
#
#   Run fluent
fluent 3d -t$ncpus -pinfiniband.ofed -cnf=pnodes -g < journal3.jou
```

Journal File for Simulation Setups

```
/file/read-case rpm45_result.cas.h5
/file/read-data rpm45_result.dat.h5

/solve/set/time-step ;timestep size
0.004
/solve/dual-time-iterate ;number of timesteps
42
20 ;iterations
/file/write-case-data rpm45_result_1.cas

exit
yes
```